 doi:10.20944/preprints202202.0044.v1



*Article*

# Early Effects of Extracellular Vesicles Secreted by Adipose Tissue Mesenchymal Cells in Renal Ischemia Followed by Reperfusion: Mechanisms Rely on the Restoration of the Redox Tissular Environment

Jarlene A. Lopes[1,2,‡], Federica Collino[1,3,‡], Clara Rodrigues-Ferreira[1,2], Luzia da Silva Sampaio[1], Glória Costa-Sarmento[1,4], Camila H.C. Wendt[1], Fernando P. Almeida[4], Kildare R. Miranda[1,4,5], Tais H. Kasai-Brunswick[2,4], Rafael S. Lindoso[1,2,4,*], Adalberto Vieyra[1,2,4,6,*]

[1] Carlos Chagas Institute of Biophysics, Federal University of Rio de Janeiro, Rio de Janeiro, Brazil jarlenelopes@biof.ufrj.br (J.A.L.); federica.collino@unimi.it (F.C.); clara_ferreira@biof.ufrj.br (C.R.F.); sampaio.lu@biof.ufrj.br (L.S.S.); sarmento@biof.ufrj.br (G.C.S.); camilawendt@biof.ufrj.br (C.H.C.W); kmiranda@biof.ufrj.br (K.R.M.); lindoso@biof.ufrj.br (R.S.L.); avieyra@biof.ufrj.br (A.V.)

[2] National Center of Science and Technology for Regenerative Medicine/REGENERA, Federal University of Rio de Janeiro, Rio de Janeiro, Brazil; jarlenelopes@biof.ufrj.br (J.A.L.); clara_ferreira@biof.ufrj.br (C.R.F.); tais@cenabio.ufrj.br (T.H.K-B.); lindoso@biof.ufrj.br (R.S.L.); avieyra@biof.ufrj.br (A.V.)

[3] Laboratory of Pediatric Nephro-urological Translational Research, Department of Clinical Sciences and Community Health, University of Milan, Milan, Italy; federica.collino@unimi.it (F.C.)

[4] National Center of Structural Biology and Bioimaging/CENABIO, Federal University of Rio de Janeiro, Rio de Janeiro, Brazil; sarmento@biof.ufrj.br (G.C.S.); fepealmeida@micro.ufrj.br (F.P.A.); kmiranda@biof.ufrj.br (K.R.M.); lindoso@biof.ufrj.br (R.S.L.); avieyra@biof.ufrj.br (A.V.)

[5] National Center of Science and Technology for Structural Biology and Bioimaging/INBEB, Federal University of Rio de Janeiro, Rio de Janeiro, Brazil; kmiranda@biof.ufrj.br (K.R.M)

[6] Graduate Program in Translational Biomedicine/BIOTRANS, Grande Rio University/UNIGRANRIO, Duque de Caxias, Brazil; avieyra@biof.ufrj.br (A.V.)

*Correspondence: lindoso@biof.ufrj.br (R.S.L.) and avieyra@biof.ufrj.br (A.V.). Carlos Chagas Institute of Biophysics, 373 Carlos Chagas Filho Ave., Federal University of Rio de Janeiro, 21941-902 Rio de Janeiro, Brazil.

‡ These authors contributed equally to this work.

 doi:10.20944/preprints202202.0044.v1



**Abstract:** Acute kidney injury (AKI) caused by ischemia followed by reperfusion (I/R) is characterized by intense anion superoxide ($O_2^{\bullet-}$) production and oxidative damage. We investigated whether extracellular vesicles secreted by adipose tissue mesenchymal cells (EVs) administrated during reperfusion can suppress the exacerbated mitochondrial $O_2^{\bullet-}$ formation after I/R. We used Wistar rats submitted to bilateral renal arterial clamping (30 min) followed by 24 h of reperfusion. The animals received EVs (I/R+EVs group) or saline, I/R group) in the kidney subcapsular space. The 3rd group was of the false-operated rats (SHAM). Mitochondria were isolated from proximal tubule cells and immediately used. Amplex Red™ was used to measure mitochondrial $O_2^{\bullet-}$ formation and MitoTracker® Orange to evaluate $\Delta\psi$. In vitro studies were carried out by using human renal proximal tubular cells (HK-2) co-cultured or not with EVs under hypoxia conditions. Administration of EVs restored $O_2^{\bullet-}$ formation to SHAM levels in all mitochondrial functional conditions. The expression of catalase and superoxide dismutase remained unmodified; transcription of heme oxygenase-1 (HO-1) was upregulated. The co-cultures of HK-2 cells with EVs revealed an intense decrease in apoptosis. We conclude that the mechanisms by which EVs recover the renal structure and function after I/R are related to the normalization of the mitochondrial redox environment. The intravesicular catalase is central in the preservation mechanisms that, with the aid of the upregulated antioxidant HO-1/Nuclear factor erythroid 2-related factor 2 system, depress early processes of cell death after I/R and open new vistas for the treatment of AKI.

***Keywords*:** extracellular vesicles; mesenchymal cells; proximal tubular cells; renal ischemia/reperfusion; mitochondria; anion superoxide; acellular therapy; regenerative medicine

HIGHLIGHTS

- Intense anion superoxide production in acute renal injury
- Mitochondria are the main source of anion superoxide
- Extracellular vesicles secreted by mesenchymal cells restore normal redox microenvironments
- Intravesicular catalase and Heme oxygenase-1/Nuclear factor erythroid 2-related factor 2 system are central in preventing oxidative damage

Preprints (www.preprints.org) | NOT PEER-REVIEWED | Posted: 3 February 2022 doi:10.20944/preprints202202.0044.v1



## 1. Introduction

Acute kidney injury (AKI) is one of the more severe systemic syndromes in internal medicine, with significant mortality rates, especially in intensive care units (ICUs), where it accounts for more than 15% of the hospitalized patients [1] and 50% of those that are critically ill [2]. The economic impact is also very high; in the United States, it is estimated that it is higher than 20 billion dollars per year [3]. Facing the controversy regarding several non-specific available treatments nowadays and the severity of the outcomes [4,5], the search for therapeutic alternatives is growing worldwide. In the last few decades, the replacements started focusing on cell therapies to prevent or slow the progression from AKI to chronic kidney disease (CKD). In the beginning, the hope was centered on renal resident adult stem cells [6,7], which was almost totally dissipated when the existence of such cells was challenged [8,9]. Now, the use of progenitor cells is intensely focused on mesenchymal stromal cells (MSC) and the vesicles they secrete to the extracellular milieu (EVs). Recently, we demonstrated that EVs secreted by adipose MSC block the progression of cellular and molecular lesions 3 days after AKI provoked by ischemia followed by reperfusion (I/R) in rats [10].

The sudden temporary impairment of renal blood flow (ischemia) followed by restoration of circulation (reperfusion) is a central event in AKI of different etiologies [11], and intense production of reactive $O_2$ species (ROS) occurs in the ischemic kidney and reoxygenation [12]. The exacerbated production of ROS – together with an important inflammatory component – is a central process in the physiopathogenesis of AKI-associate lesions as a consequence of I/R, which initiates a cascade of molecular events and aberrant signaling that culminates in tubular destruction [13], severe impairment of renal function and high mortality or frequent progress to CKD and end-stage of renal disease [14].

The early moments of the AKI onset and the response to treatments are crucial to define the evolution and prognosis [15]. Therefore, knowledge regarding the molecular and cellular events in these early and short times could support the search for appropriate therapies and their targets, especially the mechanisms altered after the burst and continuity of ROS formation. Facing the effect of EVs secreted by adipose MSC, which subcapsular administration at the beginning of reperfusion prevented or diminished tissular and functional damage 3 days after I/R [10], the present study aimed to investigate the early (24 h) EVs-induced molecular processes responsible for the late beneficial outcomes. We previously demonstrated that EVs stained with the fluorescent probe Vybrant DiD diffuse and are uniformly distributed in the kidneys 24 h

*Preprints* (www.preprints.org) | NOT PEER-REVIEWED | Posted: 3 February 2022 doi:10.20944/preprints202202.0044.v1



after their injection [10]. We hypothesized that they could modulate processes linked to preventing oxidative damage before sustained transcriptional and translation of renoprotective effects occur.

Bilateral clamping of renal arteries for 30 min was the *in vivo* model of I/R we used in rats. Specific objectives of this study were to investigate whether subcapsularly administered EVs, *i.e.*, an acellular therapeutic approach, could modulate: (**i**) renal ROS production 24 h after I/R (bilateral arterial clamping for 30 min followed by 24 h of reperfusion), (**ii**) the $O_2$ consumption in different respiratory states to dissect the influence of I/R and EVs in electron fluxes and ATP synthesis, and (**iii**) the transcriptional status of injury molecular markers, antioxidant enzymes, and pro-inflammatory cytokines. The lesional biomarkers and the plasma levels of urea and creatinine were used to determine the damage status at this moment. The effect of EVs on apoptosis was studied *in vitro* by cytometry, using cultures of an established lineage of human renal proximal tubule cells (HK-2) submitted to 24 h of hypoxia. Using this *in vitro* model, we also evaluated the electrical potential difference across the inner mitochondrial membrane ($\Delta\psi$) following the MitoTracker® Orange fluorophore distribution.

## 2. Results

### 2.1. *Characterization of extracellular vesicles secreted by adipose tissue mesenchymal stromal cells*

The mesenchymal stromal cells (MSC) secreted EVs presented in Figure 1A. They constitute a population of microvesicles (diameter above 120 nm) and exosomes (diameter ranging 50–120 nm), as demonstrated by the electron transmission microscopy (TEM) representative images. The images at higher magnification allow detecting a well-delimited membrane that encircles non-homogeneous content. In Figure 1B, the detection of surface EVs markers [16] confirm the nature of the vesicles seen in panel A, with enrichment of exosomes markers such as tetraspanins and endosomal related proteins.

### 2.2. *Mitochondria submitted to hypoxic damage are key targets for the extracellular vesicles secreted by mesenchymal cells*

Processes that contribute to the maintenance of the electrical potential difference across the inner mitochondrial membrane ($\Delta\psi$) are key for the potential

Preprints (www.preprints.org) | NOT PEER-REVIEWED | Posted: 3 February 2022 doi:10.20944/preprints202202.0044.v1



recovery of damaged cells with high metabolic demand and elevated rates of $O_2$ consumption. This is the case for renal proximal tubule cells, in which mitochondrial integrity is required for the synthesis of ATP in a nephron segment where active processes of transport, mainly of $Na^+$, take place at high rates [17]. Figure 2A demonstrates the normal mitochondrial morphology in HK-2 cells cultured in CTR conditions (*i.e.* the cells are maintained in normoxia, on the left), the appearance of pathological myelin figures in mitochondria from cells cultured in hypoxia (in the middle of the panel), and the recovery of the normal mitochondrial morphology when HK-2 cells were co-cultured with EVs (on the right). The bar graph in Figure 2B quantifies the mitochondrial area showing its decrease in hypoxia condition and the recovery of the CTR mean value when the renal cells were cultured with EVs.

Figure 2C shows representative MitoTracker® Orange labeling images (3 different magnification levels). The mitochondrial network around the nucleus is dense and intertwined with in CTR HK-2 cells (a qualitative indication of preserved $\Delta\psi$; in the left) and rarified in the cells submitted to 24 h hypoxia during 24 h (in the middle). When HK-2 cells previously exposed to 1% $O_2$ during 24 h were co-cultured for an equal period of time with EVs, the CTR mitochondrial morphology was partially recovered (in the right). Figure 2D presents the distribution of the number of events normalized to mode, which were recorded in flow cytometry analysis of HK-2 cells also stained with MitoTracker® Orange. Mean fluorescence intensity (MFI), which was also analyzed by flow cytometry, highlighted the complete overlap in the intensity measured in CTR, HPX and HPX+EVs conditions, indicating that despite the mitochondrial morphological alterations the $\Delta\psi$ is preserved under the assayed hypoxia conditions. Figure 2E (mean ± SEM) quantifies the values of mitochondrial fluorescence intensities in arbitrary units (AU). These data suggest that organization and structure of renal mitochondria could be the target of potential beneficial effects of EVs, in early stages after hypoxic injuries.

### 2.3. *Subcapsular administration of extracellular vesicles secreted by adipose tissue mesenchymal cells restores normal values of anion superoxide formation by renal mitochondria after ischemia/reperfusion*

The rates of $O_2^{\bullet-}$ formation by isolated renal mitochondria in different respiratory states have been measured in SHAM, I/R, and I/R+EVs rats after 24 h of reperfusion. Figure 3 presents representative recordings of resorufin fluorescence variations after successive additions of substrates, uncoupler, and inhibitors to mitochondria suspensions. These recordings correspond to $H_2O_2$ formation after the dismutation of

Preprints (www.preprints.org) | NOT PEER-REVIEWED | Posted: 3 February 2022 doi:10.20944/preprints202202.0044.v1



the $O_2^{\bullet-}$ that is produced as a consequence of premature transfer to $O_2$ of the electrons removed during oxidation of endogenous substrates and succinate. The comparison of Figures 3A and B allows perceiving that the velocity of $O_2^{\bullet-}$ formation increases by 50% after addition of succinate (traces between peaks 1 and 2) in mitochondria isolated from I/R rats, which returned to the SHAM value when EVs were injected at the beginning of reperfusion (Figure 3C). The quantification of the velocities when mitochondria oxidize succinate in non-phosphorylating conditions is given in Figure 3D. It can be seen that EVs treatment totally recovers the control formation of $H_2O_2$.

After adding 0.1 mM ADP, a condition in which phosphorylation to ATP occurs at lower velocity, there was no difference among the 3 groups (average of 1,000 pmol $H_2O_2 \times mg^{-1} \times min^{-1}$ over the entire period) (data not shown). When electron transfer and ATP formation were accelerated by the addition of a higher ADP concentration (1 mM) (Figure 4A), $H_2O_2$ formation decreased in the 3 groups (compare with Figure 3D) and the 50% stimulation in the I/R group with respect to SHAM appeared again, as well as the recovery of the SHAM velocity in the I/R+EVs group. A similar profile of stimulation/recovery, though at higher levels, was encountered when ATP synthesis – and respiration – was blocked by oligomycin (Figure 4B). When the respiration became accelerated and the $H^+$ electrochemical gradient dissipated by the addition of the uncoupler FCCP (Figure 4C), the $H_2O_2$ formation decreased in all groups. Still, the profile of increase by I/R and total normalization by EVs persisted. Finally, when electron fluxes were greatly diminished by inhibition of Complex III by Antimycin A, the rate of $H_2O_2$ formation increased by 100% with respect to SHAM, and the decrease promoted by EVs was partial (Figure 4D).

An interesting feature was encountered when $H^+$ leak, one of the most important mechanisms of antioxidant defense in mitochondria [18], was investigated. Proton leak in mitochondria (*i.e*. the return of $H^+$ from the interspace to the matrix through pathways different from the $F_oF_1$-ATPsintase) can be estimated from the difference between the $QO_2$ in the presence of oligomycin and the residual $QO_2$ after inhibition of Complex III by Antimycin A [19–21]. Figure 5 shows that $H^+$ leak was similar in the 3 groups and, therefore, that the ischemic episode followed by reoxygenation did not affect the pathways through which $H^+$ flow back to the matrix through pathways different from the $F_oF_1$-ATPsintase.

### 2.4. *Twenty-four hours after ischemia followed by reperfusion, the acute renal lesions still persist*

*Preprints* (www.preprints.org) | NOT PEER-REVIEWED | Posted: 3 February 2022 doi:10.20944/preprints202202.0044.v1



To see whether the early normalization of the redox status of renal cortical mitochondria was associated with amelioration of the acute lesions provoked by the ischemia followed by reperfusion, we investigated the expression of 2 biomarkers of kidney damage 24 h after the injury. They were Kidney Injury Molecule-1 (KIM-1) and Neutrophil Gelatinase-Associated Lipocalin (NGAL), which are considered sensitive and specific markers of proximal tubule lesions [22,23]. KIM-1 was barely detectable in SHAM conditions and increased approximately 20 times in the renal *cortex corticis* of I/R rats, a level that remained unmodified in the group I/R+EVs (Figure 6A). As in the case of KIM-1, the expression of NGAL was very low in SHAM rats, increasing more than 15 times after I/R without influence of EVs treatment (Figure 6B). The reminiscent pathological dysfunction of AKI is confirmed by the elevated levels of urea (87.8 ± 2.0 mg/dL *vs*. 57.8 ± 1.0 mg/dL in SHAM; $p = 0.0017$) and creatinine (0.47 ± 0.01 mg/dL *vs*. 0.28 mg/dL in SHAM; $p = 0.0001$) in blood, which were not modified by EVs administration in the 24 h window of lesion (100.3 ± 10.4 mg/dL for urea, NS with respect to I/R, $p = 0.0001$ *vs*. SHAM; 0.52 ± 0.05 mg/dL for creatinine, NS with respect to I/R, $p < 0.0001$ *vs*. SHAM) (one-way ANOVA, followed by Tukey's test; n = 5–7).

Since hypoxia and exacerbated ROS formation can trigger and positively feed inflammatory processes in kidney tubule cells and their interstitial surroundings [13], the next step was to study the expression of 2 pro-inflammatory cytokines: Interleukin-6 (IL-6) (Figure 7A) and Tumor Necrosis Factor-alpha (TNF-$\alpha$) (Figure 7B). Both cytokines were remarkably upregulated after ischemia followed by 24 h of reperfusion to 700 and 100% higher levels, respectively, with respect to SHAM values. The effects of the EVs administration were different for each cytokine, once IL-6 dropped by half compared to I/R and TNF-$\alpha$ remained unmodified in I/R+EVs rats, probably due to different influences of redox environment alterations in the release of these cytokines. This point will be discussed below.

### 2.5. *The early anti-oxidative responses after EVs administration coexist with unmodified transcriptional activation of key enzymes involved in redox regulation*

It is well known that enzyme-catalyzed antioxidant mechanisms control the balance between cell death and survival in acute renal lesions [24]. Thus we investigated the expression: (**i**) of a master regulator of cellular redox homeostasis and mitochondrial function [25,26], the heme oxygenase-1 (HO-1), and (**ii**) of 2 enzymes that catalyze the sequential split of $H_2O_2$ to $H_2O$ and $O_2$ after its formation by dismutation of $O_2^{\bullet-}$: catalase (CAT) and superoxide dismutase (SOD), respectively. The expression of HO-1 in proximal tubules increased by 300% after I/R compared to

Preprints (www.preprints.org) | NOT PEER-REVIEWED | Posted: 3 February 2022 doi:10.20944/preprints202202.0044.v1



SHAM. The upregulated levels remained unmodified by EVs injection (Figure 7C), evidence that I/R triggered an antioxidant mechanism of defense that could participate in the early restoration of the mitochondrial redox status presented in Figures 3 and 4, without any influence of the EVs content components. The profile was the opposite for CAT (Figure 7D) and SOD (Figure 7E) transcription, which was downregulated in I/R and, again without any EVs effects, indicating that I/R partially inhibited transcriptional processes unable to be restored – in the early phase of the damage – by the factors that the vesicles carry.

### 2.6. *Apoptotic processes are partially reverted when renal proximal tubule cells are co-cultured with extracellular vesicles after hypoxia*

We investigated whether EVs can prevent cell death in a lineage of kidney proximal tubule cells besides their beneficial influence in the increased redox stress. HK-2 cells submitted to hypoxia for 24 h were analyzed by Annexin/PI staining (Figure 8). Hypoxia, which mimics ischemia *in vitro*, increased the number of apoptotic cells, especially of those in late-stage, *i.e*. of $ANX^+PI^+$ cells (by approximately 3 times; Figure 8A, B, E), and by 100% the number of cells in an early stage of apoptosis ($ANX^+$) (Figure 8A, B, D). The co-culture with EVs in the reoxygenation phase significantly decreased the process of early cell death (Figure 8C, D), but not that of late apoptosis (Figure 8C, E).

## 3. Discussion

The main finding in this study was that subcapsular administration of MSC-derived EVs at the moment of reperfusion after ischemia totally recovers the normal ROS formation by mitochondria from renal proximal tubule cells in all functional respiratory states. Recovery of basal and controlled production of ROS is required for a proper mitochondrial function, including ATP synthesis and energy delivery for a varied ensemble of cell processes, especially ion transport [27], and this was achieved within 24 h after I/R by the EVs that diffused from the renal subcapsular region to the entire parenchyma, as we recently demonstrated by *in vivo* biofluorescense approaches [10].

We found that electron leak, *i.e.* the premature transfer of electrons to $O_2$ forming $O_2^{\bullet-}$ [28] is the major early mitochondrial molecular event after non-septic AKI caused by I/R. The rate of $O_2^{\bullet-}$ augmented by more than 50% after mitochondrial energization by addition of succinate, the respiratory substrate of Complex II (Figures 3 and 4), even though this complex *per se* is not a source of $O_2^{\bullet-}$ formation [29,30]. This substrate was chosen for the following reasons. First, during ischemia, the destruction

Preprints (www.preprints.org) | NOT PEER-REVIEWED | Posted: 3 February 2022 doi:10.20944/preprints202202.0044.v1



of tubule cells releases fatty acids that are oxidized, forming $FADH_2$ from FAD at the level of Complex II; when reoxygenation occurs, the electrons it carries being transferred to the Complexes III and IV. At the level of Complex III, there is an intense production of $O_2^{\bullet-}$ [29] that can be carried to the cytosol by voltage-dependent anion channels [31]. The second reason was that $O_2^{\bullet-}$ formation at the level of Complex I resulted from reverse transfer of electrons from $FADH_2$ [32], thus activating a new site for the mitochondrial generation of ROS. The importance of the EVs-induced total blockade of the uncontrolled $O_2^{\bullet-}$ production and tissue damage emerges from the observation that damage of cytosolic structures is propagated to intact mitochondria, which amplifies the vicious circle of mitochondrial destruction [33].

Of particular interest is the effect of I/R – and of EVs – when $O_2^{\bullet-}$ formation was assayed in phosphorylating conditions after the addition of 1 mM ADP (Figure 4A). The production of $O_2^{\bullet-}$ after I/R decreased to less than 15% when compared with the values obtained in the presence of succinate alone (Figure 3D), as a consequence of the dissipation of the $\Delta_{eleq}H^+$ during the simultaneous ATP synthesis [32,34]. The complete recovery of control rates of $O_2^{\bullet-}$ production points to the beneficial influence of EVs in maintaining ATP synthesis and recovering the lower velocity of $O_2^{\bullet-}$ formation, thus avoiding the amplified damage of I/R through the impairment of ATP synthesis. The similarity between the profiles in phosphorylating conditions and with FCCP (uncoupled) (Figure 4A,C) supports the view that dissipation of $\Delta_{eleq}H^+$ is the mechanism on which relies the decrease in the overall rate of $O_2^{\bullet-}$ formation. The increase by 50% of $O_2^{\bullet-}$ formation after I/R could be attributed to the intensification of the pro-oxidant microenvironment and electron leak in the vicinity of the Fe.S-containing 14 central subunits of Complex I [35], which alternate between successive cycles of oxidation/reduction during the catalysis of electron transport [36]. Possibly, the premature transfer of electrons to $O_2$ occurs to a lesser extent in Complex III, possibly because it contains fewer Fe.S centers in its dimeric structure [37].

The view of selective oxidative damage of the electron transport system as a critical early mechanism for mitochondrial dysfunction is reinforced by the observation that $O_2^{\bullet-}$ production increases by more than 80% in the I/R group in comparison with SHAM when phosphorylation was blocked by oligomycin (Figure 4B), whereas $H^+$ leak – which is estimated by the $QO_2$ in this condition and is considered a central antioxidant defense [18,21] – remained unmodified (Figure 5). Since increased $O_2^{\bullet-}$ enhances $H^+$ leak, thus favoring uncoupling, and uncoupling decreases $O_2^{\bullet-}$ [38], it may be that the lack of effects of I/R observed in Figure 5 results from protective feedback mutually involving the two processes.

Preprints (www.preprints.org) | NOT PEER-REVIEWED | Posted: 3 February 2022 doi:10.20944/preprints202202.0044.v1



The only partial recovery of the rate of $O_2^{\bullet-}$ formation in the group I/R+EVs when compared to SHAM, as well as the high acceleration caused by I/R when the ETS is blocked by Antimycin A at the level of Complex III (Figure 4D), is probably due to the complexity of the pathways for the electron fluxes when this inhibition occurs. When Complex III is blocked, the electrons flow from succinate toward Complex IV through the alternative pathway that requires high spatial organization. It involves reverse transfer of electrons to Complex I [32] that is part of the supercomplex $I_1$+$III_2$+$IV_1$ [39–41], followed by electron tunneling through the mobile pool of coenzyme Q towards Complex IV. It is likely that under intense pro-oxidant activity and lipid peroxidation, this pool is easily destructured, favoring electron leak, increasing further $O_2^{\bullet-}$ formation and impairing repair mechanisms.

The recovery of the normal mitochondrial redox status by EVs seems to be a very early process that is not accompanied by an overall improvement of the injuries caused by I/R. Neither expression of KIM-1 nor the NGAL, two key lesional biomarkers of acute renal injury, were modified by EVs (Figure 6), thus confirming that intense tubular lesions persist. Since 72 h after I/R, the expression of the tubular lesional biomarker KIM-1 was strongly downregulated in rats given EVs [10], and this was accompanied by almost normalization of the high Bcl2/Bax ratio, an indicator of mitochondrial recovery [42], it may be proposed that early preservation of a physiological redox mitochondrial microenvironment during the first 24 h of reperfusion after ischemia helped to avoid elevated lipid peroxidation and, therefore, activation of Bax-related proteins with later apoptosis. And, also, this ensemble of events occurred in the middle of extensive tubular damage, as demonstrated by the maintenance of I/R high levels of KIM-1 and NGAL after administration of EVs. In the case of NGAL, an opposite view deserves consideration. Its upregulated expression could be viewed as indicative of an antiapoptotic response that could help later recovery, as proposed for an *in vivo* endotoxin-induced model of AKI in rats [43].

Tubular damage is accompanied by the persistent inflammatory response as evidenced by the elevated levels of the cytokines IL-6 and TNF-∝ (Figure 7), which expression increased in several models of AKI [44,45]. The elevated pro-inflammatory TNF-∝, which remained unmodified in rats receiving EVs, indicates immune infiltration [46] and is probably responsible for the only partial decrease of IL-6 levels [47], which remaining amount after 24 h could contribute to reducing lipid peroxidation and oxidative damage [48]. Possibly, the partial selective early decrease of the master regulator IL-6 [49] by EVs results from the release of anti-inflammatory factors contained within the EVs that were demonstrated in our previous proteomic studies [10].

Preprints (www.preprints.org) | NOT PEER-REVIEWED | Posted: 3 February 2022 doi:10.20944/preprints202202.0044.v1



The decrease in $O_2^{\bullet-}$ in all respiratory states in the first 24 h promoted by EVs was not due to transcriptional up-regulation of the enzymes that, sequentially, catalyzes the formation of $H_2O_2$ from $O_2^{\bullet-}$ (SOD) and its conversion to $H_2O$ and $O_2$ (CAT), because their levels remain the same encountered in I/R (Figure 7D, E). These enzymes became downregulated as the ROS production increased in I/R [50–52], thus worsening the prognosis of tubular damage. It may be that the sudden decrease in the $pO_2$ during the ischemia together with the formation of $O_2^{\bullet-}$ during reperfusion resulted in the shutdown of transcription promoters [53], as demonstrated for the CAT from normal and tumoral cells from different origins, together with the destabilization of preexisting mRNA [24].

Of particular relevance is the upregulation of HO-1 by I/R, which was not modified in I/R that received EVs (Figure 7C). The mRNA levels 24 h after I/R are similar to those encountered after 72 h [10], when immunohistochemistry analysis revealed small areas positively stained for HO-1. This correlation may indicate that the upregulation of this antioxidant gene is an essential part of the early intrinsic response of kidney cells facing the oxidative stress caused by I/R. This protective response is associated to a previous step of activation of the Nuclear factor (erythroid-derived 2)-like 2 (Nrf2) and translocation to the nucleus, which is ensured by rapid, numerous, and interacting pathways [54]. Due to the role of HO-1 in the regulation of processes such as inflammation and apoptosis [26], its early upregulation without further modification by EVs appears to be central in the crossroad between apoptosis and survival collaborating with the rapid EVs-mediated protective antioxidant mechanisms in mitochondria discussed above.

The images and the bar graph in Figure 8 revealed that EVs transferred to renal cells – at least in part – the molecular machinery able to stimulate mechanisms of repair previously characterized by proteomic studies [10]. The antioxidant effects evidenced by the decrease in $O_2^{\bullet-}$ formation and upregulation of HO-1, early protective mechanisms of EVs, resulted in decreased apoptosis in renal cells cultured with EVs after they were submitted to extreme anoxia. It is worth mentioning that the upregulation of these mechanisms is related to cell survival and proliferation [55,56]. One of the key factors shuttled by EVs secreted by MSC is the catalase, whose inactivation suppresses the beneficial effects of EVs [57]. Its release after diffusion of EVs into renal parenchyma [10] could be responsible for suppressing the excess of $O_2^{\bullet-}$ formed during I/R.

In conclusion, we demonstrated that the early and central mechanism by which EVs protect the renal structure and function after I/R is the normalization of the mitochondrial redox environment. The antioxidant components of EVs are central in the

Preprints (www.preprints.org) | NOT PEER-REVIEWED | Posted: 3 February 2022 doi:10.20944/preprints202202.0044.v1



preservation mechanisms that, with the aid of the upregulated antioxidant HO-1, depress early processes of mitochondrial damage and cell death after I/R. The proposed molecular events elicited by EVs are depicted in Figure 9.

## 4. Materials and Methods

### 4.1. *Ethical statement*

All experimental procedures were approved by the Committee of Ethics in Animal Experimentation of the Federal University of Rio de Janeiro (CEUA) (protocol N° A02/16-61-15) and performed under the Committee's guidelines, following the Uniform Requirements for Manuscripts Submitted to Biomedical Journals. The animal study is reported in accordance with ARRIVE guidelines [58].

### 4.2. *Isolation and characterization of extracellular vesicles secreted by adipose mesenchymal stromal cells*

Human adipocyte mesenchymal stromal cells (MSC) were purchased from Lonza (Basel, Switzerland). They were cultured in dishes with Dulbecco´s Modified Eagle Medium (DMEM) (Life Technologies, Carlsbad, CA, USA) at 37ºC under an atmosphere of 5% $CO_2$ in air. When cells attained 80% confluence, they were washed twice with phosphate-buffered saline (PBS) at pH 7.2 and starved for 14–16 h in Roswell Park Memorial Institute (RPMI) medium without phenol red (Thermo Fisher Scientific, Waltham, MA, USA). The culture medium was then centrifuged at 1,713 × *g* for 20 min at room temperature to remove cell debris and apoptotic bodies, and the supernatant was centrifuged at 100,000 × *g* for 2 h at 4ºC. The recovered sediment contained exosomes and microvesicles (40–100 nm and 100–500 nm, respectively; Figure 1A), *i.e.*, a heterogeneous population of EVs (resuspended in 200 µL RPMI containing 1% dimethyl sulfoxide and immediately stored at -80ºC).

For the morphological characterization of the vesicles by transmission electron microscopy, the pellets obtained as above were resuspended in PBS (pH 7.2) and adhered onto glow-discharged formvar-coated copper grids (300 mesh; EMS, Hatfield, PA, USA) for 10 min. The solution´s excess was removed using filter paper (Whatman No 1; Merck, Darmstadt, Germany). Then, the grids were negatively stained with 1% (w/v) aurothioglucose in water for 30 s and dried with the same filter paper. The samples were observed on a Tecnai-Spirit electron microscope (Thermo Fisher Scientific) operating at 120 kV and equipped with a 2K camera (Veleta, Olympus, Münster, Germany).

Preprints (www.preprints.org) | NOT PEER-REVIEWED | Posted: 3 February 2022 doi:10.20944/preprints202202.0044.v1



The EVs surface antigens CD9, CD63, TSG101, and CD81, were assayed by Western blotting (Figure 1B) using the corresponding antibodies. CD9 (#ab92726, anti-rabbit, at 1:100 dilution) was from Abcam (Cambridge, United Kingdom). CD63 (#sc-5275), TSG101 (# sc-136111), and CD81 (#sc-70803) were from Santa Cruz Biotechnology (Dallas, TX, USA) (anti-mouse in the 3 cases at 1:100 dilution). The secondary antibodies were anti-rabbit (1:2,500; GE Healthcare, Cheshire, United Kingdom) and anti-mouse (1:5,000; GE Healthcare). The procedures for immunodetection were as recently described [59], except that the protein immunosignals were detected using the ImageQuant LAS 4000 system (GE Healthcare, Chicago, IL, USA).

### 4.3. *Animals and treatments*

We utilized adult male Wistar rats weighing 200–300 g available at the Central Animal Facilities Health Sciences Center, Federal University of Rio de Janeiro (Rio de Janeiro, Brazil). The animals were housed in a room and maintained at 23 ± 1$^{o}$C on a 12:12 h light-dark cycle and allowed to acclimatize during 1 week, with free access to a commercial chow for rats (Purina Agribands, Paulínia, Brazil) and filtered tap water. As stated above, the experimental protocols followed the guidelines and were approved by the local ethical committee.

The rats were randomly divided into 3 groups: (**i**) false operated (SHAM), (**ii**) ischemia/reperfusion (I/R), and (**iii**) I/R that received subcapsularly 2 × $10^9$ EVs (in 150 µL PBS) at the moment of reperfusion (I/R+EVs). The group I/R received the same volume of saline. The I/R protocol was as previously described with slight modifications [60]. Briefly, the rats were anesthetized with 0.2 mL ketamine 10% plus 0.1 mL xylazine 2% (Syntec, Santana de Parnaíba, Brazil) intraperitoneally, and the anesthesia was confirmed by pressing the posterior legs. The abdominal cavity was opened, the renal pedicles were dissected, and the renal arteries were clamped for 30 min using a stainless-steel clamp. The pedicle was smoothly manipulated in the SHAM group after visualization without dissection.

The rats received a xylocaine topical ointment and were placed in individual cages under the same previous conditions for 24 h. They were sacrificed by decapitation, and both kidneys were immediately removed. For the experiments intended for studies of reactive $O_2$ species (ROS) formation and $O_2$ consumption, the mitochondria of the external portion of the cortex (*cortex corticis*) were isolated as previously described [60] with slight modifications. In this segment of the renal tissue, more than 90% of the cell population corresponds to proximal tubules [61]. Briefly, the

Preprints (www.preprints.org) | NOT PEER-REVIEWED | Posted: 3 February 2022 doi:10.20944/preprints202202.0044.v1



cortical fragments were washed twice using a solution containing 250 mM sucrose, 10 mM Hepes-Tris (pH 7.4), 2 mM $Na_2EDTA$, and 0.15 mg/mL of trypsin inhibitor (Sigma-Aldrich, St. Louis, MO, USA), which was used in the following steps. After gentle manual homogenization using a glass Potter Elvehjem homogenizer (Merck), the total homogenates were centrifuged at 4°C. First, at 600 × *g* for 5 min to sediment intact cells, cell debris, and nuclei, recovering the supernatants that were immediately centrifuged for 10 min at 12,000 × *g* to obtain mitochondria-enriched sediments. These sediments were resuspended in 5 mL of the above-described solution and centrifuged again at 12,000 × *g* to obtain a washed pellet containing mitochondria, finally resuspended in 300 µL of the above solution and immediately used. For the experiments intended for mRNA analysis and relative quantitative expression, the whole cortex region was processed as recently described [10].

### 4.4. *Renal cells cultures and hypoxia/reoxygenation protocol*

Immortalized cells from human kidney proximal tubules (HK-2 lineage; ATCC, Manassas, VA, USA) were cultured in 6-wells plates ($5 \times 10^5$ cells per well) in Keratinocyte Serum-Free Medium (K-SFM) (Thermo Fisher Scientific) supplied with 5% (v/v) bovine fetal serum (Gibco™, Thermo Fischer Scientific), under an atmosphere of 5% $CO_2$ in air at 37°C, until they reached 80% confluence. The cells were then divided into 2 parts and cultured in serum-free DMEM, under normoxia (19% $O_2$, 5% $CO_2$ in air) or hypoxia (1% $O_2$, 5% $CO_2$ in $N_2$), at 37°C for 24 h. Next, the plates were cultured for 24 h at 37°C under normoxia. Part of the cells previously submitted to 24 h-hypoxia conditions was co-cultured with $2 \times 10^9$ EVs. Thus, we obtained 3 groups: (**i**) CTR, 24 h normoxia → 24 h normoxia; (**ii**) HPX, 24 h hypoxia → 24 h normoxia; (**iii**) HPX + EVs, 24 h hypoxia → 24 h normoxia in co-culture with EVs.

### 4.5. *Flow cytometry*

The 3 populations of HK-2 cells were detached by adding 1 mL of PBS containing 0.05% (w/v) porcine pancreatic trypsin (Trypsin-EDTA, Thermo Fischer Scientific). The cell suspensions were centrifuged at 321 × *g* for 5 min at room temperature, and the pellet-containing cells were resuspended in 100 µL of a solution containing 10 mM Hepes-Tris (pH 7.4), 140 mM NaCl and 2.5 mM $CaCl_2$ (solution C from Annexin V kit, Thermo Fischer Scientific). The samples (50 µL of the suspension) were supplied with 3 µL of Annexin V (solution A from Annexin V kit) and 3 µL of a solution containing 0.15 mM propidium iodide (10-fold diluted solution B from Annexin V kit). The cytometry analyses were carried out immediately after 15 min at room

Preprints (www.preprints.org) | NOT PEER-REVIEWED | Posted: 3 February 2022 doi:10.20944/preprints202202.0044.v1



temperature using an Accuri™ C6 flow cytometer (Accuri Cytometers Inc./Becton Dickinson, Franklin Lakes, NJ, USA). The remaining 50 µL of the cells suspensions were supplied with 50 nM of MitoTracker® Orange (Molecular Probes, Eugene, OR, USA) diluted in DMEM, incubated for 15 min, mixed with 700 µL RPMI, centrifuged at 321 × *g* for 5 min and washed 3 times with this solution. The final pellet was resuspended in 300 µL RPMI, and immediately observed in the same Accuri™ C6 flow cytometer.

### 4.6. *Analysis of mitochondrial morphology and qualitative evaluation of the electrical potential difference across the inner mitochondrial membrane from renal cells in co-culture with extracellular vesicles*

HK-2 cells were fixed in 2.5% (v/v) glutaraldehyde with 4% (v/v) formaldehyde in 0.1 M cacodylate buffer (pH 7.2) for 24 h. Following a wash in cacodylate buffer 0.1 M, the samples were post-fixed in 1% $OsO_4$ (w/v) plus 0.8% (w/v) $K_4(CN)_6Fe$ in 0.1 M cacodylate buffer for 40 min, dehydrated in acetone series and embedded in epoxide resin (Embed 812 Resin, EMS, Hatfield, PA, USA). Ultrathin sections (70 nm) were obtained using a Leica EM UC7 ultramicrotome (Leica, Wetzlar, Germany), collected onto 200 mesh copper grids (EMS), and stained for 20 min in 5% (w/v) uranyl acetate and 5 min in Reynolds' lead citrate. After, the samples were observed on a Tecnai-Spirit electron microscope (FEI Company, Eindhoven, Netherlands) operating at 120 kV, equipped with a 2k CCD camera (Veleta, Olympus). Profiles of mitochondria in randomly selected cells were evaluated with the ImageJ software (U. S. National Institutes of Health, Bethesda, Maryland, USA), and we compared the average area among the different experimental groups. Due to the polymorphic shape of the cells, we did not measure the volumetric density.

HK-2 cells were also used to qualitatively investigate the energetic mitochondrial state – represented by the transmembrane potential $\Delta\psi$ – after hypoxia and the influence of co-culture with EVs, as recently described [59]. HK-2 cells from the 3 experimental groups described above were placed in plates of 24 wells, incubated with the fluorophore MitoTracker® Orange (Molecular Probes), and assayed as follows for immunofluorescence visualization. Since the HK-2 cells do not adhere to glass, the coverslips at the bottom of the plates were washed with 400 µL Attachment Factor Cascade Biologics™ AF (Thermo Fisher Scientific) and immediately dried at 37ºC for 30 min. The cells ($8 \times 10^4$ per well, suspended in 500 µL of DMEM without serum) were placed onto 13 mm-diameter coverslips deposited at the bottom of the wells, washed twice with PBS, and supplied with 500 µL of the fluorophore diluted in a modified Krebs

Preprints (www.preprints.org) | NOT PEER-REVIEWED | Posted: 3 February 2022 doi:10.20944/preprints202202.0044.v1



solution containing 120 mM NaCl, 4 mM KCl, 1.4 mM $MgCl_2$, 2.5 mM $CaCl_2$, 6 mM glucose and 10 mM HEPES (pH adjusted to 7.4 with Tris), and incubated for 20 min at 37ºC. Then, the cells were washed 3 times for 5 min with the same solution and fixed with paraformaldehyde 4% (w/v) for 15 min at room temperature sheltered from the light. After removing the fixator, the cells were rewashed 3 times for 5 min using the same solution. The coverslips were carefully removed from the plate with the aid of a small tweezer, supplied with 20 µL of DAPI (5 µg/mL in a PBS-glycerol 40% (v/v) solution at pH 7.4 adjusted with Tris). The coverslips were mounted onto glass slides, sealed with colorless nail polish, and stored at -20ºC for 24 h. The images were collected using AxioVision 4.8.2 software in an ApoTome microscope (ApoTome Axion Imager.M2, Carl Zeiss Inc., Jena, Germany) at 554 nm (excitation) and 576 nm (emission).

### 4.7. *Time course of reactive $O_2$ species formation*

The generation of mitochondrial $O_2^{\bullet-}$ was quantified by measuring the changes in fluorescence when the fluorescent resorufin is formed by the peroxidase (2 U/mL)-catalyzed oxidation of the Amplex Red™ probe (5 mM, Thermo Fisher Scientific), after dismutation of $O_2^{\bullet-}$ into $H_2O_2$ in the presence of an excess superoxide dismutase (60 U/mL, Sigma-Aldrich), as recently described [62]. Generation of $O_2^{\bullet-}$ was evaluated at different respiratory states after substrates-uncoupler-inhibitor-titration (SUIT): (**i**) 10 mM succinate (substrate for Complex II); (**ii**) 0.1 mM ADP; (**iii**) 1 mM ADP; (**iv**) 0.2 µg/mL oligomycin (to inhibit ATP formation and to stimulate $H^+$ leak); (**v**) 1.5 µM carbonyl cyanide-4-(trifluoromethoxy) phenylhydrazone (FCCP) to completely dissipate the $H^+$ gradient; (**vi**) 2.5 µM antimycin to inhibit Complex III. The basic reaction medium before SUIT contained: 10 mM Hepes-Tris at pH 7.4, 320 mM mannitol, 4 mM $KH_2PO_4$, 4 mM $MgCl_2$, 0.08 mM $Na_2EDTA$, 1 mM EGTA (free acid) and 1 mg/mL fatty acids free BSA. The final pH was adjusted to 7.4 by adding Tris; the mitochondrial protein concentration was 0.1 mg/mL. Recordings were acquired at 563 nm (excitation) and 587 nm (emission). Calibration curves were obtained using successive pulses of 10 nM $H_2O_2$, thus allowing the conversion of arbitrary fluorescence units in pmol $H_2O_2$/mg per min. The stoichiometry 1 $O_2^{\bullet-}$:1 $H_2O_2$ allowed quantification of $O_2^{\bullet-}$ formation rate.

### 4.8. *Oxygen consumption by isolated mitochondria from kidney proximal tubule cells*

We measured oxygen consumption ($QO_2$) by isolated mitochondria using a high-resolution $O_2$ electrode (Oxygraph-2K, OROBOROS Instruments, Innsbruck, Austria) at 37ºC in the solution above descript for mitochondrial $O_2^{\bullet-}$ determination,

Preprints (www.preprints.org) | NOT PEER-REVIEWED | Posted: 3 February 2022 doi:10.20944/preprints202202.0044.v1



except that the components required to detect $H_2O_2$ formation were omitted and 0.06 mg/mL mitochondrial protein was used. The $QO_2$ assays were run in parallel with $H_2O_2$ assays. All mitochondrial preparations were assayed to determine the respiratory control ratio (RCR) and, therefore, to evaluate the coupling between electron fluxes and ATP synthesis. The RCR was calculated from the ratio between the $QO_2$ in the presence of 1 mM ADP and the $QO_2$ after the addition of oligomycin. Despite differences in the absolute values of $QO_2$ (lower in I/R mitochondria), the RCR averaged 3.0 in all groups, with an interassay variation coefficient of ~10%. The $QO_2$ after successive additions of oligomycin and Antimycin A was used to estimate the $H^+$ leak from the mitochondrial space back to the matrix [19–21].

### 4.9. *RNA isolation, reversal transcription and real time quantitative polymerase chain reaction (qRT-PCR)*

Small fragments of kidney cortex were suspended in 500 µL of Lysis/binding buffer (miRNA isolation kit *mir*Vana™, Thermo Fisher Scientific) in RNAse-free microtubes and homogenized using the dissociator TissueLyser LT provided with a 5 mm-diameter bead (Qiagen, Hilden, Germany). After 7 min of intense agitation, 400 µL of the homogenates aliquots were mixed with 40 µL of miRNA homogenate additive (miRNA isolation kit *mir*Vana™), vigorously vortexed, and then placed on ice for 10 min. The suspensions were then supplied with the same volume of chloroform, vortexed again at 12,000 × *g* during 5 min at room temperature, to recover supernatants that were mixed with 100% ethanol (1.25 mL ethanol:1 mL sample), kindly homogenized with the use of a micropipette and centrifuged at 12,000 × *g* during 15 s at room temperature using microtubes supplied with the filter provided by the kit (miRNA isolation kit *mir*Vana™). After removing the liquid, the filters were first washed with 700 µL of the miRNA wash solution 1, centrifuged during 15 s at 12,000 × *g* at room temperature, and then washed twice using 500 µL of the miRNA wash solution 2/3 (both solutions from the kit mentioned above). Finally, the filters were immersed in 100 µL of free-RNAse $H_2O$ at 95ºC immediately centrifuged for 30 s at 13,000 × *g,* and the liquids, after removal of the filters, were stored at -80ºC.

The mRNAs were obtained using 10 µL of the High-Capacity cDNA Reverse Transcription kit (Applied Biosystems™, Foster City, CA, USA) – which components were freshly mixed – and 10 µL-samples containing 20 ng/µL mRNA. The RNA of these samples was quantified using the NanoDrop™ ND-1000 (Thermo Fisher Scientific), as recently described [10]. The cDNAs were synthesized in the thermocycler PCR Thermal Cycler (Applied Biosystems™), with cycles of 10 min at

Preprints (www.preprints.org) | NOT PEER-REVIEWED | Posted: 3 February 2022 doi:10.20944/preprints202202.0044.v1



25ºC, 120 min at 37ºC, 5 min at 85ºC, and 1 min at 4ºC, before storage at -20ºC. Negative controls without reverse transcriptase were carried out in parallel with each run.

The reversal transcription followed by the real-time quantitative polymerase chain reaction was performed in a single step using 10 µL of Power SYBR Green® PCR Master Mix (Applied Biosystems™) and 10 µL of the cDNA-containing solution and the primers (0.25 ng/µL and 100 nM, respectively). The sequence-specific oligonucleotides [10] were from Eurofins Genomics (Ebersberg, Germany) (Table 1). Their amplifications were followed using the ViiA™ 7 Real-Time System (Applied Biosystems™) after a stage of 10 min to reach 95ºC, followed by cycles of 15 min at 95ºC, 60 min at 60ºC and 15 min at 95ºC.

### 4.10. *Statistical analysis*

The mean values of the different parameters investigated in the 3 experimental groups of rats and in the 3 HK-2 cells assays were analyzed using one-way ANOVA followed by Tukey's test. In the case of RQ data, the mean of each SHAM group was taken as 1.0, and the individual values from the 3 groups were expressed as a fraction or as a multiple of this value [63,64]. This allowed the SEM of the unitary value of SHAM reference to be calculated.

**Author Contributions:** JAL, FC, RSL and AV designed the study (conceptualization). JAL, FC, CR-F, LSS, GC-S, CHCW, FPA, THK-B and RSL conducted the experiments (methodology and investigation). JAL, FC, CR-F, LSS, GC-S, CHCW, FPA, KRM, THK-B, RSL and AV analyzed and interpreted the data (validation). JAL, FC, CR-F, THK-B, RSL and AV wrote the manuscript (original draft, review and editing). AV: funding, project administration, and supervision. All authors contributed to the discussion and final version of the article and approved the submitted version.

**Funding:** This work was supported by grants from the Carlos Chagas Filho Rio de Janeiro Research State Foundation/FAPERJ (Nº E-26/202.963/2017, E-26/200.866/2021 and E-26/202.312/2021), the Brazilian National Research Council/CNPq (Nº 311578/2019-5), and the National Institute of Science and Technology for Regenerative Medicine/REGENERA (Nº 465656/2014-5). JAL received fellowships from the Brazilian National Research Council/CNPq (Nº 131942/2017-4)

 doi:10.20944/preprints202202.0044.v1



and from the Coordination for the Improvement of Higher Education Personnel/CAPES (88887.463960/2019-0).

**Institutional Review Board Statement:** The Committee of Ethics in Animal Experimentation of the Federal University of Rio de Janeiro (CEUA) (protocol N° A02/16-61-15) approved the animal study protocols.

**Informed Consent Statement:** Not applicable.

**Data Availability Statement:** The raw data supporting the conclusions of this article will be made available by the authors, without undue reservation.

**Acknowledgements**: The technical assistance by Danilo S. Alves-Bezerra is acknowledged. The access to the advanced microscopy facilities at the National Center of Structural Biology and Bioimaging/CENABIO is specially appreciated.

**Conflicts of Interest:** The authors declare that the research was conducted in the absence of any commercial or financial relationships that could represent potential conflicts of interest.

**References**

1. Pieretti, J.C.; Junho, C.V.C; Carneiro-Ramos, M.S.; Seabra, A.B. $H_2S$- and NO-releasing gasotransmitter platform: a crosstalk signaling pathway in the treatment of acute kidney injury. *Pharmacol Res*. **2020**, 161, 105121. doi: 10.1016/j.phrs.2020.105121.
2. Neyra, J.A.; Leaf, D.E. Risk prediction models for acute kidney injury in critically Ill patients: opus in progressu. *Nephron*. ***2018***, 140, 99–104. doi: 10.1159/000490119.
3. Silver, S.A.; Chertow, G.M. The economic consequences of acute kidney injury. *Nephron*. **2017**, 137, 297–301. doi: 10.1159/000475607.
4. Wang, A.Y.; Bellomo, R. Renal replacement therapy in the ICU: intermittent hemodialysis, sustained low-efficiency dialysis or continuous renal replacement therapy? *Curr Opin Crit Care.* **2018**, 24, 437–42. doi: 10.1097/MCC.0000000000000541.

5. Iacovella, G.M.; Kumar, N. Controversies surrounding renal replacement therapy in the critically Ill patient. *Semin Respir Crit Care Med.* **2019**, 40, 662–72. doi: 10.1055/s-0039-1697966.
6. Oliver, J.A. Adult renal stem cells and renal repair. *Curr Opin Nephrol Hypertens.* **2004**, 13, 17–22. Doi: 10.1097/00041552-200401000-00003.
7. Bussolati, B.; Bruno, S.; Grange, C.; Buttiglieri, S.; Deregibus, M.C.; Cantino, D.; Camussi, G. Isolation of renal progenitor cells from adult human kidney. *Am J Pathol.* **2005**, 166, 545–55. doi: 10.1016/S0002-9440(10)62276-6.
8. Humphreys, B.D.; Valerius, M.T.; Kobayashi, A.; Mugford, J.W.; Soeung, S.; Duffield, J.S.; McMahon, A.P.; Bonventre, J.V. Intrinsic epithelial cells repair the kidney after injury. *Cell Stem Cell.* **2008**, 2, 284–91. doi: 10.1016/j.stem.2008.01.014.
9. Kusaba, T.; Lalli, M.; Kramann, R.; Kobayashi, A.; Humphreys, B.D. Differentiated kidney epithelial cells repair injured proximal tubule. *Proc Natl Acad Sci U S A.* **2014**, 111, 1527–32. doi: 10.1073/pnas.1310653110.
10. Collino, F.; Lopes, J.A.; Corrêa, S.; Abdelhay, E.; Takiya, C.M.; Wendt, C.H.C.; de Miranda, K.R.; Vieyra, A.; Lindoso, R.S. Adipose-derived mesenchymal stromal cells under hypoxia: changes in extracellular vesicles secretion and improvement of renal recovery after ischemic injury. *Cell Physiol Biochem.* **2019**, 52, 1463–83. doi: 10.33594/000000102.
11. Han, S.J.; Lee, H.T. Mechanisms and therapeutic targets of ischemic acute kidney injury. *Kidney Res Clin Pract.* **2019**, 38, 427–40. doi: 10.23876/j.krcp.19.062.
12. Baud, L.; Ardaillou, R. Involvement of reactive oxygen species in kidney damage. *Br Med Bull.* **1993**, 49, 621–29. doi: 10.1093/oxfordjournals.bmb.a072635.
13. Mulay, S.R.; Holderied, A.; Kumar, S.V.; Anders, H.J. Targeting inflammation in so-called acute kidney injury. *Semin Nephrol.* **2016**, 36, 17–30. doi: 10.1016/j.semnephrol.2016.01.006.
14. Fortrie, G.; de Geus, H.R.H.; Betjes, M.G.H. The aftermath of acute kidney injury: a narrative review of long-term mortality and renal function. *Crit Care.* **2019**, 24, 24. doi: 10.1186/s13054-019-2314-z.
15. Bhatraju, P.K.; Zelnick, L.R.; Chinchilli, V.M.; Moledina, D.G.; Coca, S.G.; Parikh, C.R.; Garg, A.X.; Hsu, C.Y.; Go, A.S.; Liu, K.D.; *et a*l. Association between early recovery of kidney function after acute kidney injury and long-term clinical outcomes. *JAMA Netw Open.* 2020, 3, e202682. doi: 10.1001/jamanetworkopen.2020.2682.
16. Willms, E.; Johansson, H.J.; Mäger, I.; Lee, Y.; Blomberg, K.E.; Sadik, M.; Alaarg, A.; Smith, C.I.; Lehtiö, J.; El Andaloussi, S.; Wood, M.J.; Vader, P. Cells release

subpopulations of exosomes with distinct molecular and biological properties. *Sci Rep.* **2016**, 6, 22519. doi: 10.1038/srep22519.

17. Knox, F.G.; Fleming, J.S.; Rennie, D.W. Effects of osmotic diuresis on sodium reabsorption and oxygen consumption of kidney. *Am J Physiol.* **1966**, 210, 751–9. doi: 10.1152/ajplegacy.1966.210.4.751.
18. Nanayakkara, G.K.; Wang, H.; Yang, X. Proton leak regulates mitochondrial reactive oxygen species generation in endothelial cell activation and inflammation - A novel concept. *Arch Biochem Biophys.* **2019**, 662, 68–74. doi: 10.1016/j.abb.2018.12.002.
19. Nicholls, D.G. The influence of respiration and ATP hydrolysis on the proton-electrochemical gradient across the inner membrane of rat-liver mitochondria as determined by ion distribution. *Eur J Biochem.* **1974**. 50, 305–15. doi: 10.1111/j.1432-1033.1974.tb03899.x.
20. Nicholls, D.G. Mitochondrial membrane potential and aging. *Aging Cell.* **2004**, 3, 35–40. doi: 10.1111/j.1474-9728.2003.00079.x.
21. Brand, M.D.; Nicholls, D.G. Assessing mitochondrial dysfunction in cells. *Biochem J*. **2011**, 435, 297–312. doi: 10.1042/BJ20110162.
22. Bonventre, J.V. Kidney Injury Molecule-1 (KIM-1): a specific and sensitive biomarker of kidney injury. *Scand J Clin Lab Invest Suppl.* **2008**, 241, 78–83. doi: 10.1080/00365510802145059.
23. Devarajan, P. Neutrophil gelatinase-associated lipocalin (NGAL): a new marker of kidney disease. *Scand J Clin Lab Invest Suppl.* **2008**, 241, 89–94. doi: 10.1080/00365510802150158.
24. Glorieux, C.; Zamocky, M.; Sandoval, J.M.; Verrax, J.; Calderon, P.B. Regulation of catalase expression in healthy and cancerous cells. *Free Radic Biol Med.* **2015**, 87, 84–97. doi: 10.1016/j.freeradbiomed.2015.06.017.
25. Lever, J.M.; Boddu, R.; George, J.F.; Agarwal, A. Heme oxygenase-1 in kidney health and disease. *Antioxid Redox Signal.* **2016**, 25, 165–83. doi: 10.1089/ars.2016.6659.
26. Loboda, A.; Damulewicz, M.; Pyza, E.; Jozkowicz, A.; Dulak, J. Role of Nrf2/HO-1 system in development, oxidative stress response and diseases: an evolutionarily conserved mechanism. *Cell Mol Life Sci.* **2016**, 73, 3221–47. doi: 10.1007/s00018-016-2223-0.
27. Gonzalez-Vicente, A.; Hong, N.; Garvin, J.L. Effects of reactive oxygen species on renal tubular transport. *Am J Physiol Renal Physiol.* **2019**, 317, F444–55. doi: 10.1152/ajprenal.00604.2018.

 doi:10.20944/preprints202202.0044.v1




28. Jastroch, M.; Divakaruni, A.S.; Mookerjee, S.; Treberg, J.R.; Brand, M.D. Mitochondrial proton and electron leaks. *Essays Biochem.* **2010**, 47, 53–67. doi: 10.1042/bse0470053.
29. Brand, M.D.; Buckingham, J.A.; Esteves, T.C.; Green, K.; Lambert, A.J.; Miwa, S.; Murphy, M.P.; Pakay, J.L.; Talbot, D.A.; Echtay, K.S. Mitochondrial superoxide and aging: uncoupling-protein activity and superoxide production. *Biochem Soc Symp.* **2004**, 71203–13. doi: 10.1042/bss0710203.
30. Murphy, M.P. How mitochondria produce reactive oxygen species. *Biochem J.* **2009**, 417, 1–13. doi: 10.1042/BJ20081386.
31. Lustgarten, M.S.; Bhattacharya, A.; Muller, F.L.; Jang, Y.C.; Shimizu, T. Shirasawa, T.; Richardson, A.; Van Remmen, H. Complex I generated, mitochondrial matrix-directed superoxide is released from the mitochondria through voltage dependent anion channels. *Biochem Biophys Res Commun.* **2012**, 422, 515–21. doi: 10.1016/j.bbrc.2012.05.055.
32. Dröse, S. Differential effects of complex II on mitochondrial ROS production and their relation to cardioprotective pre- and postconditioning. *Biochim Biophys Acta.* **2013**, 1827, 578–87. doi: 10.1016/j.bbabio.2013.01.004.
33. Hekimi, S.; Wang, Y.; Noë, A. Mitochondrial ROS and the effectors of the intrinsic apoptotic pathway in aging cells: the discerning killers!. *Front Genet.* **2016**, 7, 161. doi: 10.3389/fgene.2016.00161.
34. Robb, E.L.; Hall, A.R.; Prime, T.A.; Eaton, S.; Szibor, M.; Viscomi, C.; James, A.M.; Murphy, M.P. Control of mitochondrial superoxide production by reverse electron transport at complex I. *J Biol Chem.* **2018**, 293, 9869–79. doi: 10.1074/jbc.RA118.003647.
35. Zhu, J.; Vinothkumar, K.R.; Hirst, J. Structure of mammalian respiratory complex I. *Nature.* **2016**, 536, 354–58. doi: 10.1038/nature19095.
36. Wirth, C.; Brandt, U.; Hunte, C.; Zickermann, V. Structure and function of mitochondrial complex I. *Biochim Biophys Acta.* **2016**, 1857, 902–14. doi: 10.1016/j.bbabio.2016.02.013.
37. Iwata, S.; Lee, J.W.; Okada, K.; Lee, J.K.; Iwata, M.; Rasmussen, B.; Link, T.A.; Ramaswamy, S.; Jap, B.K. Complete structure of the 11-subunit bovine mitochondrial cytochrome bc1 complex. *Science.* **1998**, 281, 64–71. doi: 10.1126/science.281.5373.64.
38. Brookes, P.S.; Yoon, Y.; Robotham, J.L.; Anders, M.W.; Sheu, S.S. Calcium, ATP, and ROS: a mitochondrial love-hate triangle. *Am J Physiol Cell Physiol.* **2004**, 287, C817–33. doi: 10.1152/ajpcell.00139.2004.

39. Lenaz, G.; Genova, M.L. Structure and organization of mitochondrial respiratory complexes: a new understanding of an old subject. *Antioxid Redox Signal.* **2010**, 12, 961–1008. doi: 10.1089/ars.2009.2704.
40. Lapuente-Brun, E.; Moreno-Loshuertos, R.; Acín-Pérez, R.; Latorre-Pellicer, A.; Colás, C.; Balsa, E.; Perales-Clemente, E.; Quirós, P.M.; Calvo, E.; Rodríguez-Hernández, M.A.; *et al*. Supercomplex assembly determines electron flux in the mitochondrial electron transport chain. *Science.* **2013**, 340, 1567–70. doi: 10.1126/science.1230381.
41. Milenkovic, D.; Blaza, J.N.; Larsson, N.G.; Hirst, J. The enigma of the respiratory chain supercomplex. *Cell Metab.* **2017**, 25, 765–76. doi: 10.1016/j.cmet.2017.03.009.
42. Luo, X.; O'Neill, K.L.; Huang, K. The third model of Bax/Bak activation: a Bcl-2 family feud finally resolved? *F1000Research.* **2020**, (F1000 Faculty Review), 935. doi: 10.12688/f1000research.25607.1.1.
43. Han, M.; Li, Y.; Wen, D.; Liu, M.; Ma, Y.; Cong, B. NGAL protects against endotoxin-induced renal tubular damage by suppressing apoptosis. *BMC Nephrol.* **2018**, 19, 168.doi 10.1186/s12882-018-0977-3.
44. Faubel, S.; Lewis, E.C.; Reznikov, L.; Ljubanovic, D.; Hoke, T.S.; Somerset, H.; Oh, D.J.; Lu, L.; Klein, C.L.; Dinarello, C.A.; Edelstein, C.L. Cisplatin-induced acute renal failure is associated with an increase in the cytokines interleukin (IL)-1beta, IL-18, IL-6, and neutrophil infiltration in the kidney. *J Pharmacol Exp Ther.* **2007**, 322, 8–15. doi: 10.1124/jpet.107.119792.
45. Zhang, M.Z.; Yao, B.; Yang, S.; Jiang, L.; Wang, S.; Fan, X.; Yin, H.; Wong, K.; Miyazawa, T.; *et al*. CSF-1 signaling mediates recovery from acute kidney injury. *J Clin Invest.* **2012**, 122, 4519–32. doi: 10.1172/JCI60363.
46. Ramseyer, V.D.; Garvin, J.L. Tumor necrosis factor-α: regulation of renal function and blood pressure. *Am J Physiol Renal Physiol.* **2013**, 304, F1231–42. doi: 10.1152/ajprenal.00557.2012.
47. Shalaby, M.R.; Waage, A.; Espevik, T. Cytokine regulation of interleukin 6 production by human endothelial cells. *Cell Immunol.* **1989**, 121, 372–82. doi: 10.1016/0008-8749(89)90036-1.
48. Nechemia-Arbely, Y.; Barkan, D.; Pizov, G.; Shriki, A.; Rose-John, S.; Galun, E.; Axelrod, J.H. IL-6/IL-6R axis plays a critical role in acute kidney injury. *J Am Soc Nephrol.* **2008**, 19, 1106–15. doi: 10.1681/ASN.2007070744.
49. Su, H.; Lei, C.T.; Zhang C. Interleukin-6 signaling pathway and its role in kidney disease: an update. *Front Immunol.* **2017**, 8, 405. doi: 10.3389/fimmu.2017.00405.

 doi:10.20944/preprints202202.0044.v1




50. Paller, M.S.; Hoidal, J.R.; Ferris, T.F. Oxygen free radicals in ischemic acute renal failure in the rat. *J Clin Invest.* **1984**, 74, 1156–64. doi: 10.1172/JCI111524.
51. Baliga, R.; Ueda, N.; Walker, P.D.; Shah, S.V. Oxidant mechanisms in toxic acute renal failure. *Am J Kidney Dis.* **1997**, 29, 465–77. doi: 10.1016/s0272-6386(97)90212-2.
52. Gyurászová, M.; Gurecká, R.; Bábíčková, J.; Tóthová, Ľ. Oxidative stress in the pathophysiology of kidney disease: implications for noninvasive monitoring and identification of biomarkers. *Oxid Med Cell Longev.* **2020**, 2020, 5478708. doi: 10.1155/2020/5478708.
53. Cowan, D.B.; Weisel, R.D.; Williams, W.G.; Mickle, D.A. The regulation of glutathione peroxidase gene expression by oxygen tension in cultured human cardiomyocytes. *J Mol Cell Cardiol.* **1992**, 24, 423–33. doi: 10.1016/0022-2828(92)93196-q.
54. Bryan, H.K.; Olayanju, A.; Goldring, C.E.; Park, B.K. The Nrf2 cell defence pathway: Keap1-dependent and -independent mechanisms of regulation. *Biochem Pharmacol.* **2013**, 85, 705–17. doi: 10.1016/j.bcp.2012.11.016.
55. Wagner, E.F.; Nebreda, A.R. Signal integration by JNK and p38 MAPK pathways in cancer development. *Nat Rev Cancer.* **2009**, 9, 537–49. doi: 10.1038/nrc2694.
56. Vigolo, E.; Markó, L.; Hinze, C.; Müller, D.N.; Schmidt-Ullrich, R.; Schmidt-Ott, K.M. Canonical BMP signaling in tubular cells mediates recovery after acute kidney injury. *Kidney Int.* **2019**, 95, 108–122. doi: 10.1016/j.kint.2018.08.028.
57. de Godoy, M.A.; Saraiva, L.M.; de Carvalho, L.R.P.; Vasconcelos-Dos-Santos, A.; Beiral, H.J.V.; Ramos, A.B.; Silva, L.R.P.; Leal, R.B.; Monteiro, V.H.S.; Braga, C.V.; de Araujo-Silva, C.A.; *et al.* Mesenchymal stem cells and cell-derived extracellular vesicles protect hippocampal neurons from oxidative stress and synapse damage induced by amyloid-β oligomers. *J Biol Chem.* **2018**, 293, 1957–75. doi: 10.1074/jbc.M117.807180.
58. Percie du Sert, N.; Hurst, V.; Ahluwalia, A.; Alam, S.; Avey, M.T.; Baker, M.; Browne, W.J.; Clark, A.; Cuthill, I.C.; *et al*., The ARRIVE guidelines 2.0: updated guidelines for reporting animal research. *J Physiol.* **2020**, 598, 3793–801. doi: 10.1113/JP280389.
59. Collino, F.; Lopes, J.A.; Tapparo, M.; Tortelote, G.G.; Kasai-Brunswick, T.H.; Lopes, G.M.C.; Almeida, D.B.; Skovronova, R.; Wendt, C.H.C.; Miranda, K.R.; *et al*. Extracellular vesicles derived from induced pluripotent stem cells promote renoprotection in acute kidney injury model. *Cells.* **2020**, 9, 453. doi: 10.3390/cells9020453.

 doi:10.20944/preprints202202.0044.v1



60. Beiral, H.J.; Rodrigues-Ferreira, C.; Fernandes, A.M.; Gonsalez, S.R.; Mortari, N.C.; Takiya, C.M.; Sorenson, M.M.; Figueiredo-Freitas, C.; Galina, A.; Vieyra, A. The impact of stem cells on electron fluxes, proton translocation, and ATP synthesis in kidney mitochondria after ischemia/reperfusion. *Cell Transplant.* **2014**, 23, 207–20. doi: 10.3727/096368912X659862.
61. Whittembury, G.; Proverbio, F. Two modes of Na extrusion in cells from guinea pig kidney cortex slices. *Pflugers Arch.* **1970**, 316, 1–25. doi: 10.1007/BF00587893.
62. Bianco, M.; Lopes, J.A.; Beiral, H.J.V.; Filho, J.D.D.; Frankenfeld, S.P.; Fortunato, R.S.; Gattass, C.R.; Vieyra, A.; Takiya, C.M. The contralateral kidney presents with impaired mitochondrial functions and disrupted redox homeostasis after 14 days of unilateral ureteral obstruction in mice. *PLoS One.* **2019**, 14, e0218986. doi: 10.1371/journal.pone.0218986.
63. Sahajpal, V.; Ashton, N. Increased glomerular angiotensin II binding in rats exposed to a maternal low protein diet in utero. *J Physiol.* **2005**, 563, 193–201. doi: 10.1113/jphysiol.2004.078642.
64. Silva, P.A.; Muzi-Filho, H.; Pereira-Acácio, A.; Dias, J.; Martins, J.F.; Landim-Vieira, M.; Verdoorn, K.S.; Lara, L.S.; Vieira-Filho, L.D.; Cabral, E.V.; *et al*. Altered signaling pathways linked to angiotensin II underpin the upregulation of renal Na(+)-ATPase in chronically undernourished rats. *Biochim Biophys Acta.* **2014**, 1842, 2357–66. doi: 10.1016/j.bbadis.2014.09.017.

*Preprints* (www.preprints.org) | NOT PEER-REVIEWED | Posted: 3 February 2022 doi:10.20944/preprints202202.0044.v1



## Legends to Figures

**Figure 1.** Characterization of extracellular vesicles (EVs) secreted by adipose mesenchymal cells. (A) Morphological characterization. Electron transmission microscopy at the two indicated magnifications. (B) Characterization by using vesicular surface antigens. The immunodetections show that the EVs, which images are presented in (A), are $CD9^+$, $CD63^+$, $TSG101^+$, and $CD81^+$, as indicated.

**Figure 2.** Evaluation of structural mitochondria damage after AKI and EVs treatment. (A) Transmission electron microscopy images of mitochondria from HK-2 cells in CTR, HPX and HPX+EVs conditions, as indicated above the panels. Arrowhead in HPX points to a typical myelin figure. (B) Quantification of the mitochondrial areas. Bars represent mean ± SEM (n = 34, 37, 30 areas for CTR, HPX and HPX+EVs groups, respectively). (C) Representative fluorescence images of MitoTracker® Orange (red areas) to evaluate mitochondrial $\Delta\psi$ in CTR, HPX, and HPX+EVs. Nuclei are stained in blue (DAPI). Magnifications are indicated on the left side of the panels. The insets in the 100x magnification pictures are presented just below the panels. (D) The percentage of events in cytometry analyses (normalized to mode) at the arbitrary fluorescence intensity units indicated on the *abscissa.* The small colored squares indicate the experimental conditions: orange, CTR; blue, HPX; red, HPX+EVs. The histograms of CTR, HPX and HPX+EVs overlap. (E) The mitochondrial mean fluorescence intensities (MFI) of MitoTracker® Orange were quantified from the groups indicated on the *abscissa.* Scatter plots represent determinations in which median values of fluorescence were recorded. In (B) and (E), differences were assessed using one-way ANOVA followed by Tukey's test. (B, E) ***$P < 0.001$; ****$P < 0.0001$; NS: not significant.

*Preprints* (www.preprints.org) | NOT PEER-REVIEWED | Posted: 3 February 2022 doi:10.20944/preprints202202.0044.v1



**Figure 3.** Generation of $O_2^{\bullet-}$ in renal mitochondria 24 h after ischemia/reperfusion (I/R). Representative time courses of $H_2O_2$ formation from the $O_2^{\bullet-}$ generated in renal *cortex corticis* mitochondria during different respiratory states, which were elicited by successive additions of substrates/inhibitors. (A) SHAM rats. (B) I/R conditions. (C) I/R+EVs; EVs were injected at the beginning of reperfusion. The numbers (spikes) indicate additions to the medium. 1: 10 mM succinate; 2: 0.1 mM ADP; 3: 1 mM ADP; 4: 0.2 µg/ml oligomycin; 5: 1.5 µM FCCP; 6: 2.5 µM antimycin A. The insets allow a better comparison of the rate of formation of $H_2O_2$ over 2 min after the addition of succinate. The dismutation reaction $2O_2^{\bullet-} + 2H^+ \rightarrow H_2O_2 + O_2$ was non-limiting because an excess of superoxide dismutase (SOD) (60 U/mL) was added to the reaction medium. Standard curves were obtained by successive additions of 10 nM $H_2O_2$ pulses at 2 min time intervals, thereby allowing calculation of rates in pmol $H_2O_2 \times mg^{-1} \times min^{-1}$ (see the following figure). (D) Quantification of the $H_2O_2$ formation after addition of succinate (insets). Bars are mean ± SEM; n = 7 (SHAM); n = 7 (I/R); n = 5 (I/R+EVs). Means were compared using one-way ANOVA followed by Tukey´s test. ****$P$ < 0.0001; NS: not significant.

**Figure 4.** Quantification of $H_2O_2$ formation (energization with succinate) 24 h after I/R. Assays were carried out in the different respiratory states indicated on the *abscissae*. (A) Phosphorylating (1 mM ADP). (B) Non-phosphorylating (oligomycin). (C) Uncoupled (FCCP). (D) Residual (antimycin A). Experimental groups are also indicated on the *abscissae*. Bars indicate mean ± SEM of the number of determinations indicated in the legend to Figure 3. *$P$ < 0.05; **$P$ < 0.01; ***$P$ < 0.001; ****$P$ < 0.0001; NS: not significant (one-way ANOVA followed by Tukey´s test).

**Figure 5.** Proton leak ($QO_2$ measured in the presence of oligomycin). The reaction medium was that used to determine the production of reactive $O_2$ species in Figure 3, without adding of the components required for the formation of $H_2O_2$. The bars correspond to mean ± SEM of 6 (SHAM and I/R) and 5 (I/R+EVs) determinations with different mitochondrial preparations. Groups are those indicated on the *abscissae*. No differences were found among the 3 groups (one-way ANOVA followed by Tukey´s test).

*Preprints* (www.preprints.org) | NOT PEER-REVIEWED | Posted: 3 February 2022 doi:10.20944/preprints202202.0044.v1



**Figure 6.** The expression (relative quantification) of the renal injury biomarkers 24 h after I/R are not modified by EVs. (A) KIM-1. (B) NGAL. The expression of the enzymes was investigated from total RNA extracted from *cortex corticis*. The bars represent mean ± SEM that were compared using one-way ANOVA followed by Tukey's test. The experimental groups are indicated on the *abscissae*; n = 4 (SHAM), n = 7 (I/R), n = 5 (I/R+EVs), for both biomarkers. ****$P < 0.0001$; NS: not significant.

**Figure 7.** Expression of pro-inflammatory cytokines and antioxidant enzymes, which expression was investigated from the total RNA extracted from *cortex corticis*. (A) IL-6. (B) TNF-α. (C) Heme oxygenase-1. (D) Catalase. (E) Superoxide dismutase-1. Bars represent mean ± SEM that were compared using one-way ANOVA followed by Tukey's test. Groups are indicated on the *abscissae*; n = 4 (SHAM), n = 7 (I/R), n = 5 (I/R+EVs). *$P < 0.05$; **$P < 0.01$; ***$P < 0.001$; ****$P < 0.0001$; NS: not significant.

**Figure 8.** Co-culture with EVs decreases apoptosis of a lineage of proximal tubule cells (HK-2 line) subjected to hypoxia. Representative cytometry analysis of $3 \times 10^5$ HK-2 cells cultivated in 1.5 mL of DMEM without serum during 24 h. (A) Cultures in normoxia (CTR). (B) Hypoxia (1% $O_2$) (HPX) in the absence of EVs. (C) HPX in the presence of $2 \times 10^9$ EVs (HPX+EVs. Then the cells were incubated for 24 h under 21% $O_2$ in the same medium. (D–F) Quantification of cell death is expressed as a percent of total cells. (D) Early apoptosis, corresponding to $ANX^+PI^-$ cells. (E) Late apoptosis, corresponding to $ANX^+PI^+$ cells. (F) Sum of the cells that suffered early and late death: $ANX^+PI^-$ cells + $ANX^+PI^+$ cells. Bars represent mean ± SEM of different cultures in the conditions CTR (n = 16), HPX (n = 14) and HPX+EVs (n = 9). *$P < 0.05$; **$P < 0.01$; ***$P < 0.001$; NS: not significant (one-way ANOVA followed by Tukey´s test.

 doi:10.20944/preprints202202.0044.v1



**Figure 9.** Suppressing the excess of $O_2^{\bullet-}$: Proposed mechanisms for the rapid effects of EVs (24 h of reperfusion after renal ischemia). Mesenchymal cells (MSCs) secrete EVs that, after subcapsular administration and diffusion into the renal parenchyma [10], reach the tubular segments injured by I/R. By releasing several factors, including the catalase they carry [57], they contribute to maintaining the normal local redox state existing in the absence of injury. With mitochondrial and cytoplasmic redox homeostasis restored, the mitochondrial processes required for ATP synthesis are preserved and, therefore, the appropriate ATP supply is preserved for the transport demands and maintenance of tubular structures.

Preprints (www.preprints.org) | NOT PEER-REVIEWED | Posted: 3 February 2022 doi:10.20944/preprints202202.0044.v1



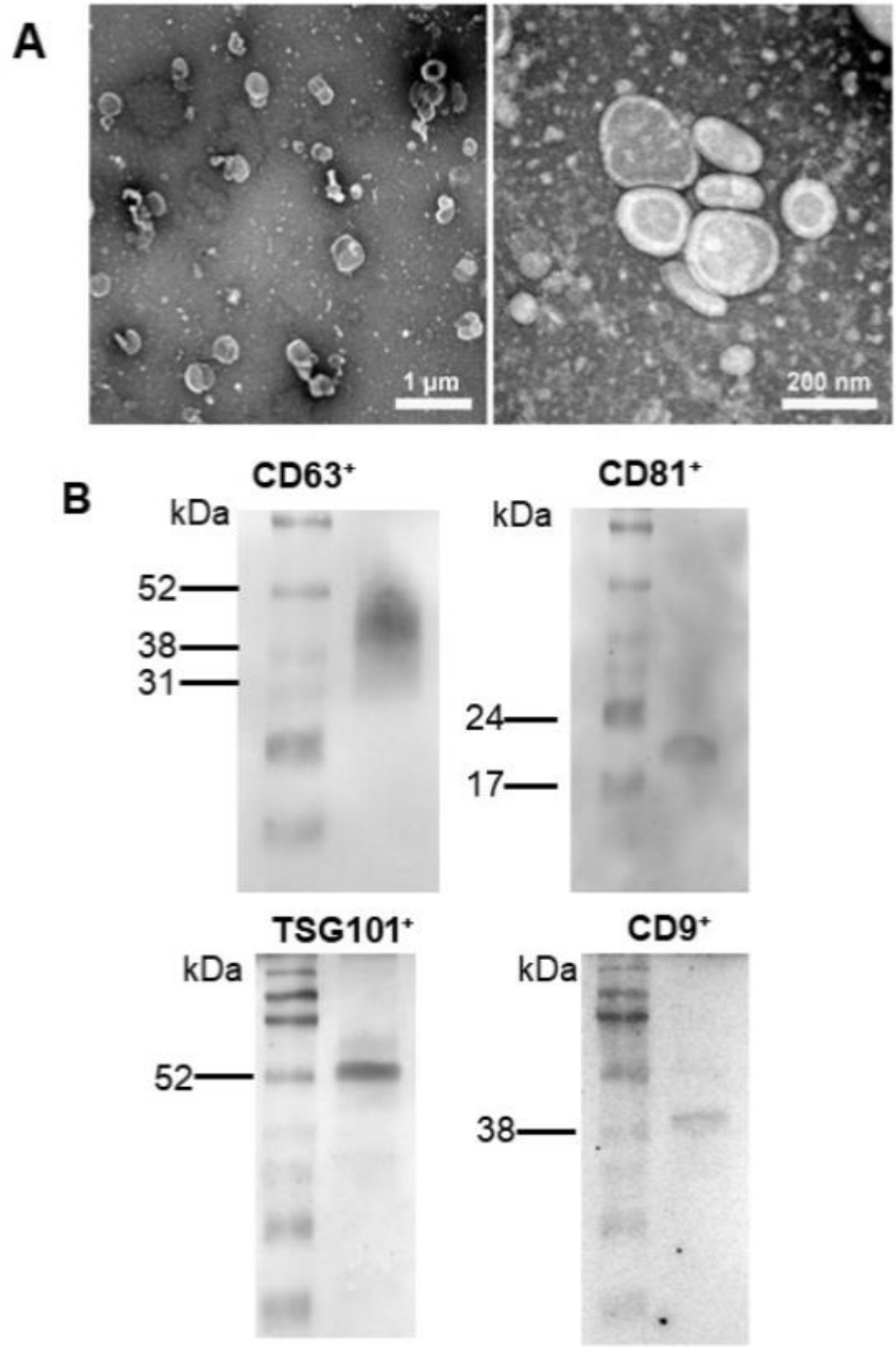


**Figure 1.**

Preprints (www.preprints.org) | NOT PEER-REVIEWED | Posted: 3 February 2022 doi:10.20944/preprints202202.0044.v1



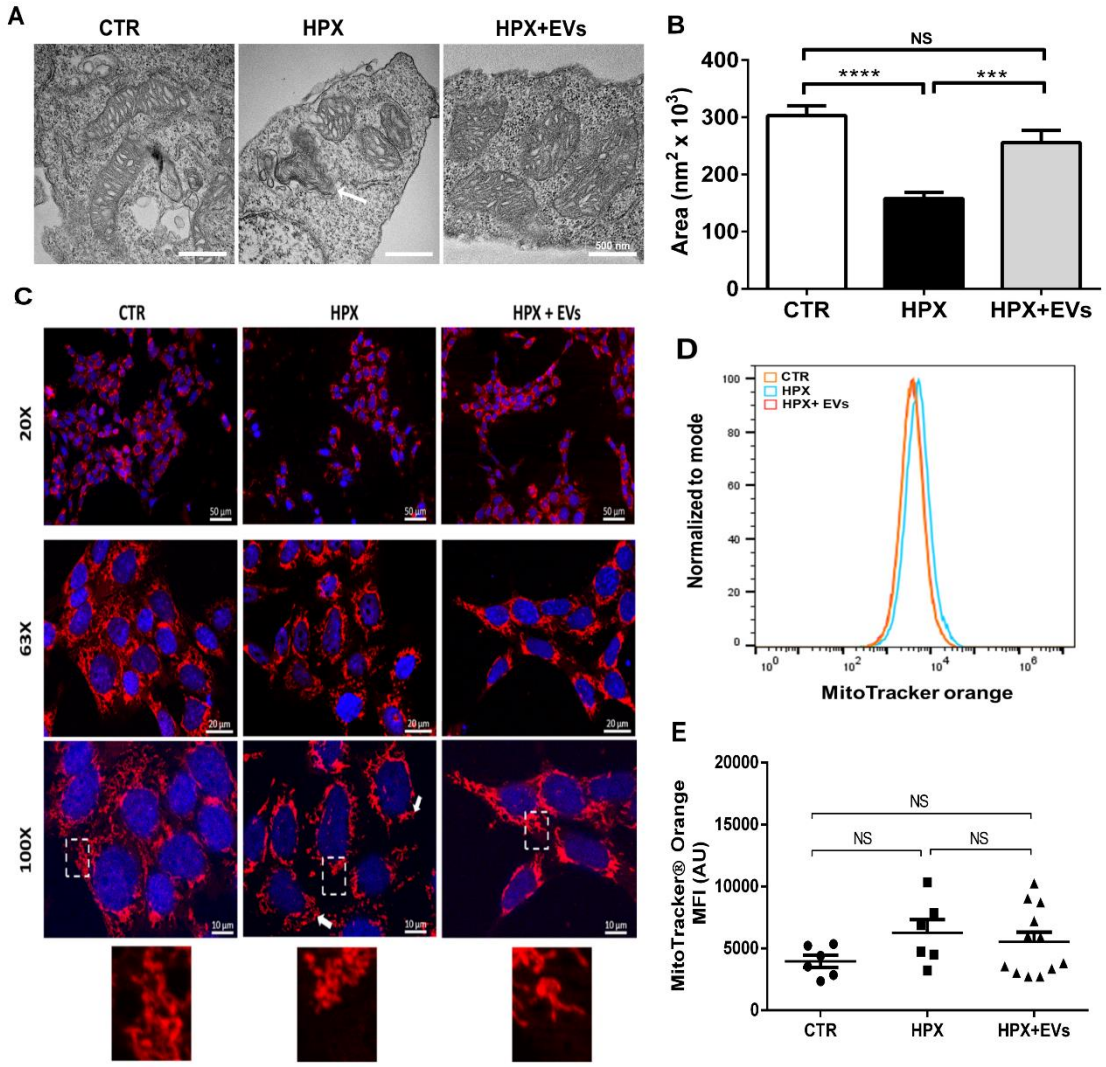


**Figure 2.**

Preprints (www.preprints.org) | NOT PEER-REVIEWED | Posted: 3 February 2022 doi:10.20944/preprints202202.0044.v1



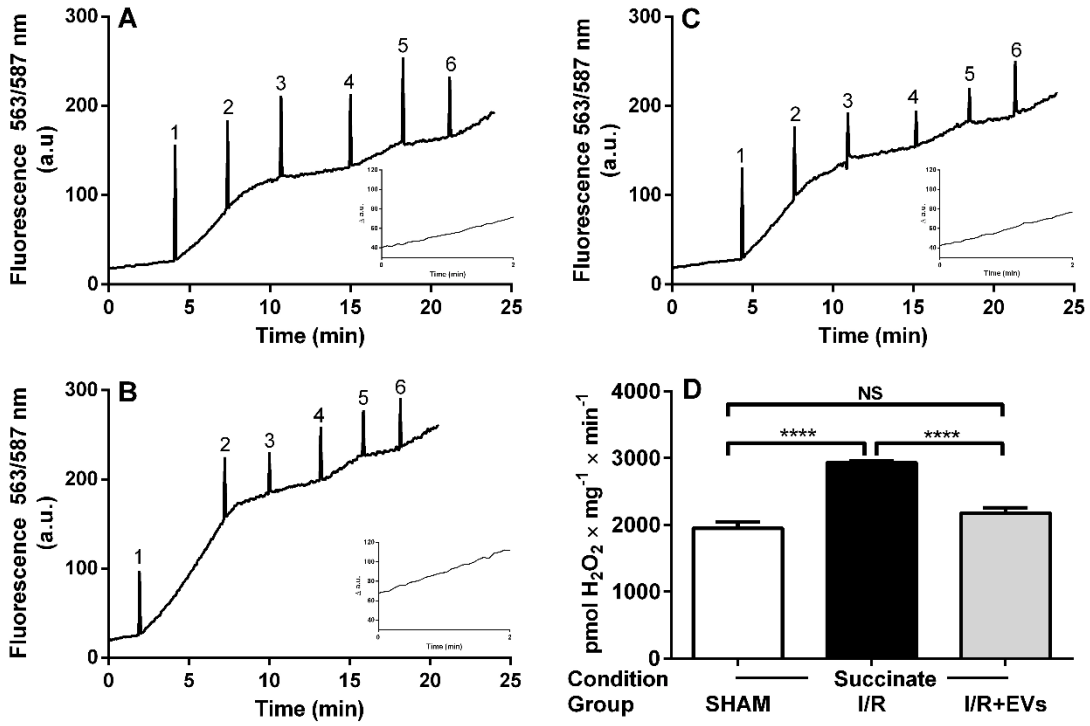


**Figure 3.**

Preprints (www.preprints.org) | NOT PEER-REVIEWED | Posted: 3 February 2022 doi:10.20944/preprints202202.0044.v1



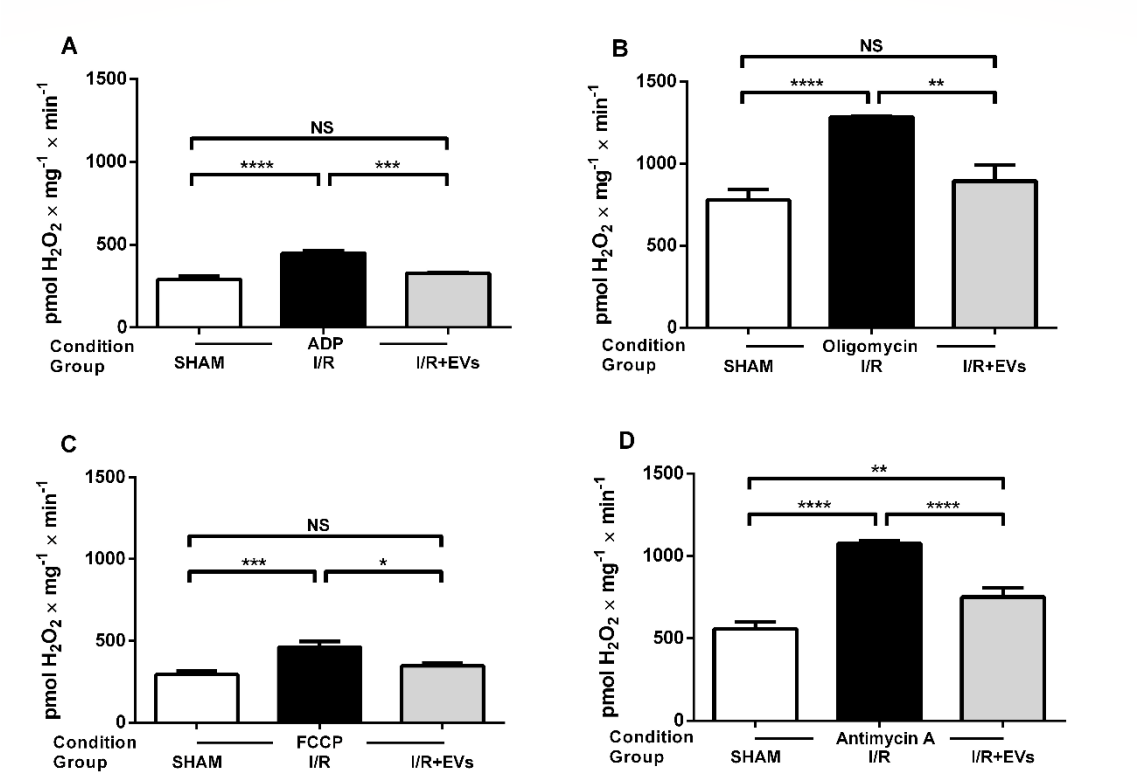


**Figure 4.**

Preprints (www.preprints.org) | NOT PEER-REVIEWED | Posted: 3 February 2022 doi:10.20944/preprints202202.0044.v1



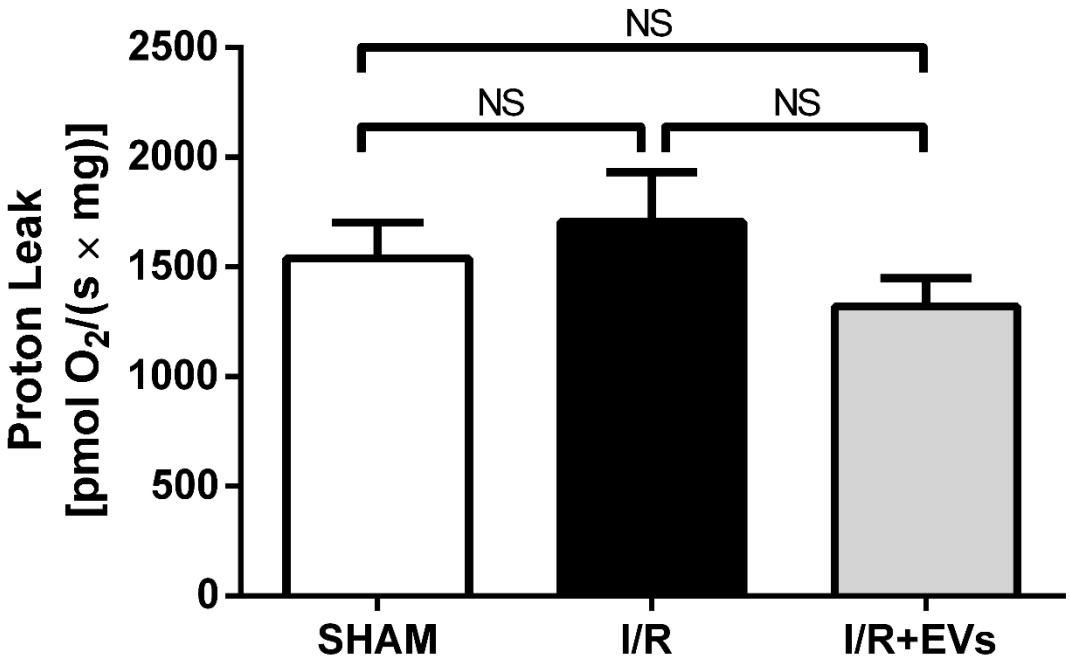


**Figure 5.**

Preprints (www.preprints.org) | NOT PEER-REVIEWED | Posted: 3 February 2022 doi:10.20944/preprints202202.0044.v1



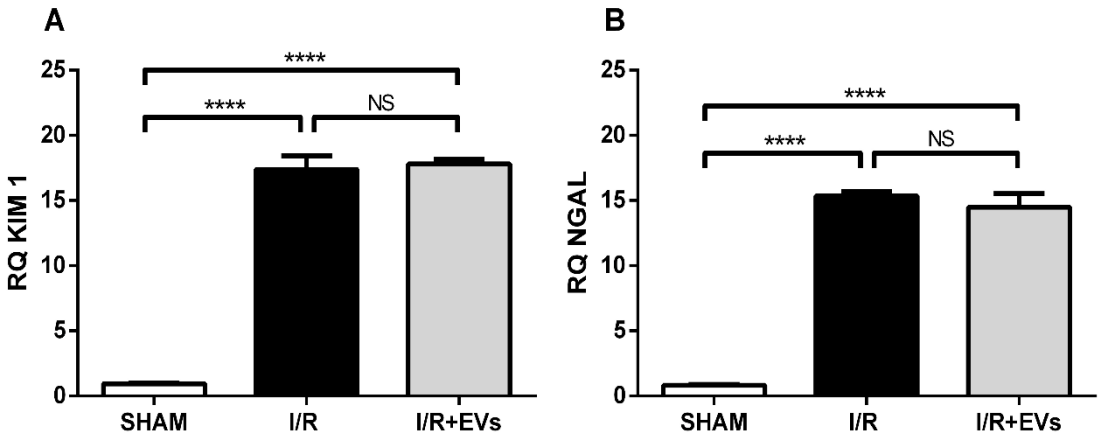


**Figure 6.**

Preprints (www.preprints.org) | NOT PEER-REVIEWED | Posted: 3 February 2022 doi:10.20944/preprints202202.0044.v1



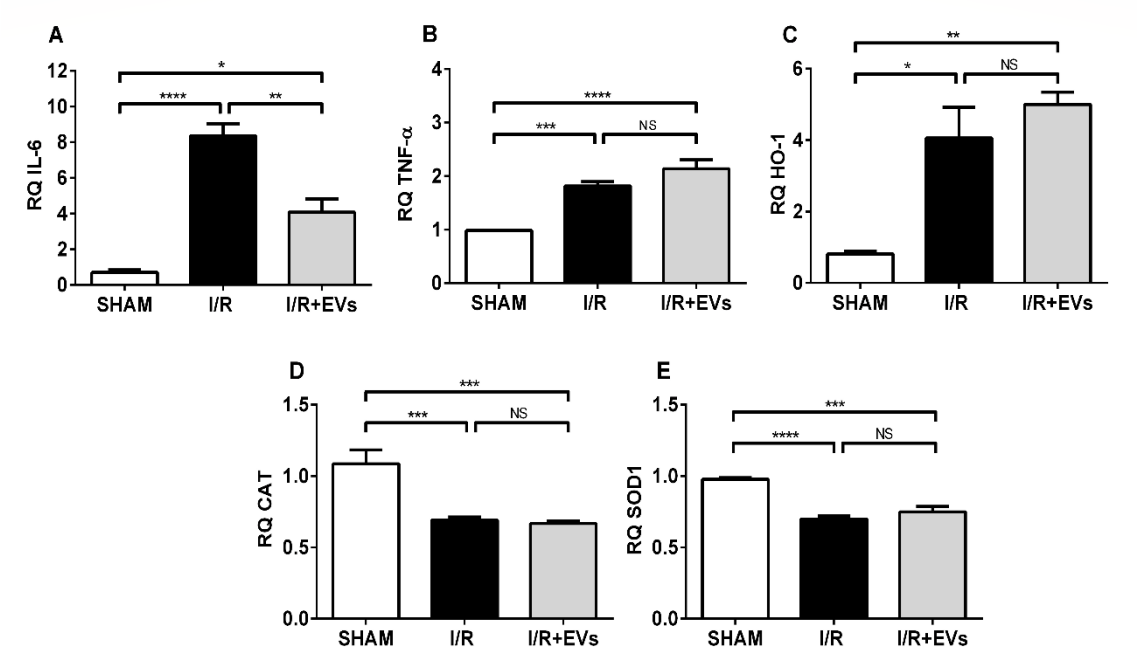


**Figure 7.**

Preprints (www.preprints.org) | NOT PEER-REVIEWED | Posted: 3 February 2022 doi:10.20944/preprints202202.0044.v1



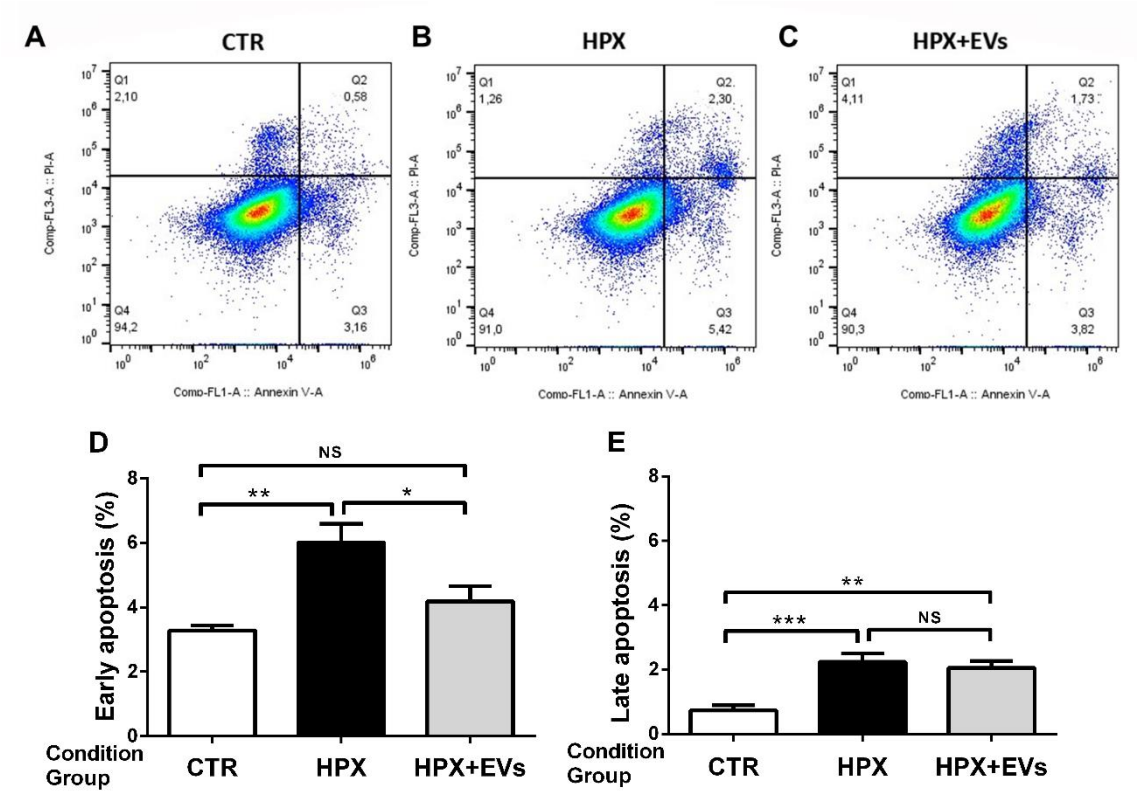


**Figure 8.**

Preprints (www.preprints.org) | NOT PEER-REVIEWED | Posted: 3 February 2022 doi:10.20944/preprints202202.0044.v1



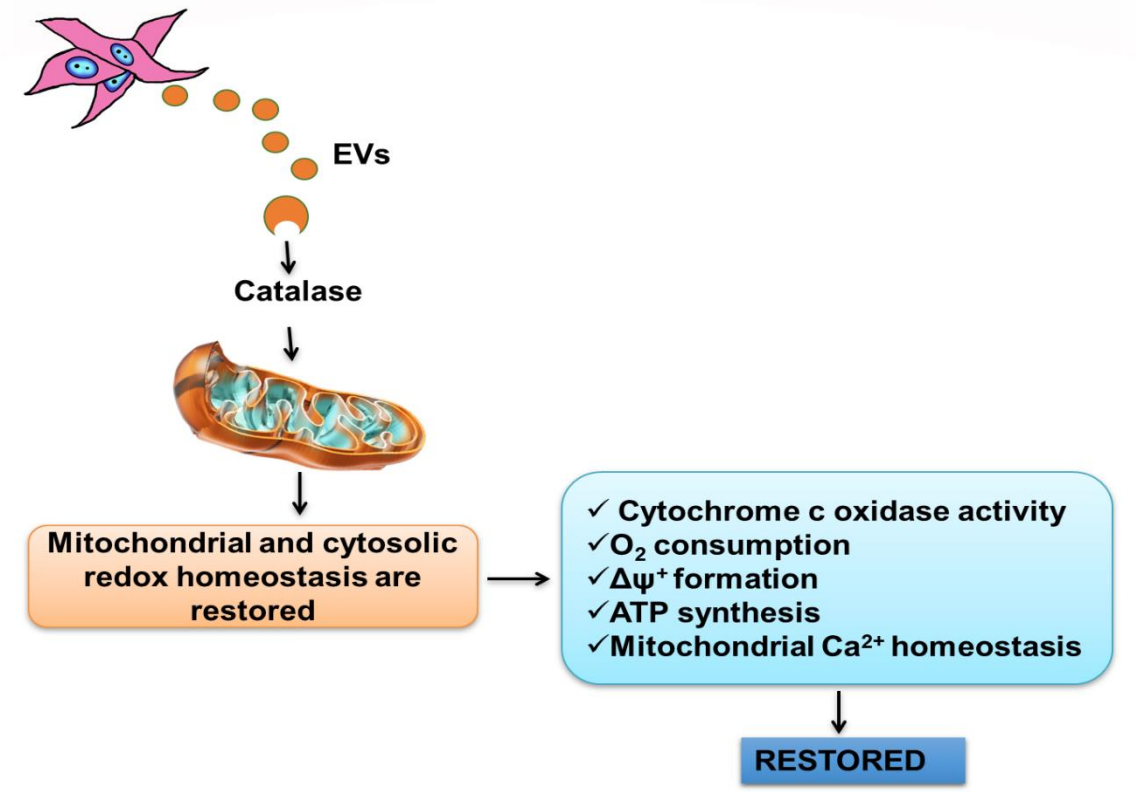


**Figure 9.**

Preprints (www.preprints.org) | NOT PEER-REVIEWED | Posted: 3 February 2022 doi:10.20944/preprints202202.0044.v1



**Table 1**. List of the primers used in qRT-PCR analysis.

| mRNA | Sequence |
|---|---|
| **r SOD1 F1** | AAGAGAGGCATGTTGGAGACC |
| **r SOD1 R1** | ACGGCCAATGATGGAATGCT |
| **r CAT F1** | CAGCTCCGCAATCCTACACC |
| **r CAT R1** | GGACATCGGGTTTCTGAGGG |
| **r IL-6 F1** | AAGCCAGAGTCATTCAGAGC |
| **r IL-6 R1** | GTCCTTAGCCACTCCTTCTG |
| **r TNFA F1** | CTTCTCATTCCTGCTCGTGG |
| **r TNFA R1** | TGATCTGAGTGTGAGGGTCTG |
| **r KIM1 F1** | ACCTGATCAGACAGAGTGTGC |
| **r KIM1 R1** | ATCTACAGAGCCTGGAAGAAGCA |
| **r HO-1 F1** | AGGTGCACATCCGTGCAGAG |
| **r HO-1 R1** | CTTCCAGGGCCGTATAGATATGGTA |
| **r NGAL F1** | GGGCTGTCCGATGAACTGAA |
| **r NGAL R1** | CATTGGTCGGTGGGAACAGA |
| **r GAPDH F1** | GCCAAAAGGGTCATCATCTC |
| **r GAPDH R1** | GGCCATCCACAGTCTTCT |